Contribution to the numerical simulation of radiative hydrodynamics

Emmanuel Labourasse

HABILITATION TO CONDUCT RESEARCH

in Mathematics

presented at

Sorbonne University

Contribution to the numerical simulation of radiative hydrodynamics

Author: Emmanuel Labourasse

Examiners:

Rémi Abgrall	University of Zurich, Professor
Michael Dumbser	University of Trento, Professor
Chi-Wang Shu	Brown University, Professor

Jury members:

Rémi Abgrall	University of Zurich, Professor
Xavier Blanc	University of Paris, Professor
Christophe Chalons	University of Paris-Saclay, Professor
Bruno Després	Sorbonne University, Professor
Michael Dumbser	University of Trento, Professor
Pierre-Henri Maire	CEA, Research Director
Chi-Wang Shu	Brown University, Professor

Defence date: December 17 2021

Acknowledgements

First, I would like to thank the three researchers who reported my work. Rémi Abrgrall, Michaël Dumbser and Chi-Wang Shu. Each of them has more significant contributions in numerical analysis than many mathematics labs. It is a great honor to have them as reviewers.

A big thank you to Christophe Chalons and Pierre-Henri Maire, who gave me the pleasure and the honor to accept to participate in my jury. I hope I will have the opportunity to work with you soon.

Without a doubt, Bruno Després has had a significant role in my scientific career. He is a magician and continues to amaze me with his creativity. As his name suggests, Xavier Blanc is the bearer of light. He dispels the deepest darkness, making everything luminous.

Thank you to Pierre Sagaut and Olivier Pironneau, my first referents in the research world. They taught me a lot. Many thanks to Olivier Lebaigue, Benoit Mathieu and Adrien Toutant my brillant collaborators during my Post-Doc.

Among my outstanding colleagues and nevertheless friends, a special mention goes to Stéphane DP. We entered the CEA/DAM simultaneously, and he was always available to help out. It is gratifying to work with him. Gilles is much more than the person who shares my office. When I first joined the company, he helped me understand the expectations of the position. Working with him is very informative... and demanding, as his standards are high.

Thank you to my successive managers, who pushed me to take this step: Bruno Scheurer, Hervé Jourdren, Pierre-Franck Piserchia and Stéphane Jaouen, without forgetting Daniel Bouche and Laurence Bonnet.

Many thanks also to Pierre, Patricia, Guillaume C, Alexandra, Laurent, Théo, Bruno, Frédéric D, Cédric, Christophe, Emmanuel, François, Philippe H, Stéphane J, Mohamed, Frédéric L, Franck L, Isabelle, Guillaume M, Julie, Gérald, Franck S, Marc, working with you is a pleasure.

Thank you for all the informal discussions and good times spent with Rémi, Nicolas, Ulrich, Fabrice, Jérome B, Jean-François, Benoît, Jérome M, Nathanael, Marie-Pierre, Robert, Philippe, Xavier R, Xavier V, and many others. Maybe we can convert it sooner or later into collaborations.

Many thanks to Alain, Céline and Françoise for their help and good mood.

I acknowledge my deep friends, Marc, Soizic, David, Arnaud, Delphine, Nicolas, Marielle, Cédric, Anne and Yann, for the power to disconnect me.

Finally, thanks to my wife Solène who has put up with me for, say, 21 years, my brothers Raphaël (38 years) and Gabriel (43 years), and my parents, Eulalia and Jean, for 47 years. You are my talents.

To Margot and Éloïse

Contents

Introduction

To describe the research I have done at CEA DAM, I consider a system of equations that serves as a guideline for this manuscript. This is the simplest model for radiation hydrodynamics that can be formulated, and consists of an assembly of the non-relativistic Euler system of equations with a non-linear radiation diffusion operator called the Rosseland diffusion model (or equilibrium diffusion). This model is sufficient to present my work, even if its scope extends to more complex models, such as non-equilibrium grey radiative hydrodynamics, or multi-group radiative hydrodynamics (the interested reader may refer to one of the reference works [Castor, 2004, Chandrasekhar, 1950, Mihalas and Weibel-Mihalas, 1999, Pomraning, 1979] or [Zel'dovich and Raizer, 1966] for a hierarchy of radiation hydrodynamics models).

The model considered here is valid within the limits of the very small optical depths (opaque materials), and in the event that the thermal conduction is negligible compared to radiative scattering. It is further assumed that the fluid velocity is non-relativistic, but large enough that the kinematic viscosity of the fluid is negligible (implying an infinite Reynolds number). A derivation of this model is available for example in [Mihalas and Weibel-Mihalas, 1999], p.460. Under these hypotheses, we can write the radiative hydrodynamics equations in integral form on a moving domain at arbitrary speed $\mathbf{u}_a$ (arbitrary Lagrange Euler - ALE), whose solutions are sought in the space of functions with bounded variations $BV(\Omega)$

$$\frac{d}{dt}\int_{\omega(t)} 1 - \int_{\omega(t)} \nabla\cdot\mathbf{u}_a = 0, \tag{1}$$

$$\frac{d}{dt}\int_{\omega(t)} \rho + \int_{\omega(t)} \nabla\cdot\rho(\mathbf{u}-\mathbf{u}_a) = 0, \tag{2}$$

$$\frac{d}{dt}\int_{\omega(t)} \rho\mathbf{u} + \int_{\omega(t)} \nabla\cdot\rho(\mathbf{u}-\mathbf{u}_a)\otimes\mathbf{u} + \int_{\omega(t)} \nabla p_T = \mathbf{0}, \tag{3}$$

$$\frac{d}{dt}\int_{\omega(t)} \rho E + \int_{\omega(t)} \nabla\cdot\rho(\mathbf{u}-\mathbf{u}_a)E + \int_{\omega(t)} \nabla\cdot p_T\mathbf{u} = \int_{\omega(t)} \nabla\cdot k\nabla T^4, \tag{4}$$

where $\omega(t)\subset\Omega(t)$ is any open subset of the fluid domain $\Omega(t)$ with a regular boundary $\mathcal{C}^1$, moving at the velocity $\mathbf{u}_a$, and in which the unknowns are sufficiently regular[1]. This system is formally identical to that of the Euler equations in integral formulation, except for the radiative diffusion $\int_{\omega(t)}\nabla\cdot k\nabla T^4$ in the energy equation. Furthermore, the pressure considered is the sum of the material pressure p and the radiative pressure $p_r=\frac{1}{3}aT^4$ (where a is the radiative density constant), and the total energy density E is the sum of the internal, kinetic and radiative energy densities ($E=e+\frac{1}{2}\mathbf{u}^2+aT^4\tau$, where $\tau=\frac{1}{\rho}$). To close the system, it is necessary to provide an equation of state that links p, T and k to e and ρ. We can then define the entropy η which follows the Gibbs law:

$$Td\eta = d\left(e+aT^4\tau\right) + p_T d\tau. \tag{5}$$

The diffusion term in the energy equation can be rewritten as a heat flow $\nabla\cdot k\nabla T^4 = \nabla\cdot K\nabla T$

[1] In the case of BV solution, these equations must rigorously be written in weak form. We allow ourselves this abuse of notation, which has no influence on the continuation of the manuscript.

where $K = 4kT^3$. The associated Clausius-Duhem inequality is then written as follows

$$\forall \omega(t) \subset \Omega(t), \quad \frac{d}{dt}\int_{\omega(t)} \rho\eta + \int_{\omega(t)} \nabla \cdot \rho(\mathbf{u} - \mathbf{u}_a)\eta \geq \int_{\omega(t)} \nabla \cdot \frac{K}{T}\nabla T. \tag{6}$$

Using Reynolds' theorem and multiplying by $T > 0$, we obtain a local form of this inequality, equivalent for regular solutions

$$\rho T \frac{D}{Dt}\eta \geq T\nabla \cdot \frac{K}{T}\nabla T. \tag{7}$$

Finally, substituting (5) in (7), yields

$$\rho \frac{D}{Dt}\left(e + aT^4\tau\right) + p_T \rho \frac{D}{Dt}\tau \geq T\nabla \cdot \frac{K}{T}\nabla T. \tag{8}$$

Alternatively, the left-hand side of (8) can be calculated using the system (1)-(4)

$$\rho \frac{D}{Dt}\left(e + aT^4\tau\right) + p_T \rho \frac{D}{Dt}\tau = \nabla \cdot K\nabla T. \tag{9}$$

By combining the equations (9) and (8) one obtains the constraint

$$\frac{K}{T}\nabla T \cdot \nabla T \geq 0. \tag{10}$$

That requires $K \geq 0$ and then $k \geq 0$. In summary, the physical solutions of this system verify

1. $\rho > 0$,
2. $k \geq 0$,
3. $T > 0$,
4. and (6),

which, with the exception of condition 2 and the form of the entropy inequality, corresponds to the invariant domain of the Euler equations (see for example [Serre, 1987, Frid, 2001]). It is physically relevant to split the entropy of the system $\eta = \eta_m + \eta_r$ into two parts, between the matter entropy η_m and the radiative entropy η_r. Each of these entropies follows its own Gibbs law

$$Td\eta_m = de + pd\tau, \tag{11}$$

$$Td\eta_r = d\left(aT^4\tau\right) + p_r d\tau. \tag{12}$$

It follows that η_r is simply defined (up to a constant) as a function of T and ρ

$$\eta_r = \frac{4}{3}aT^3\tau. \tag{13}$$

The system (1)-(4) is obviously non-linear, in particular because of the convective terms characteristic of Euler equations, but also because K depends on T and ρ. This makes the analysis and direct resolution of this system complex. This is why we have chosen to split it into three phases (fractional step method).

Phase I : hydrodynamics in the Lagrangian frame.

Phase II : Radiative diffusion with frozen hydrodynamics.

Phase III : change of frame.

This decomposition amounts to solving three successive systems of conservation laws, the initial condition of a system of equations being given by the resolution of the previous system.

Phase I The Phase I equations are formally the same as the Euler equations, but the definition of the constituent terms is slightly different. $\forall \omega(t) \subset \Omega(t)$,

$$\frac{d}{dt}\int_{\omega(t)} 1 = \int_{\omega(t)} \nabla \cdot \mathbf{u}, \tag{14}$$

$$\frac{d}{dt}\int_{\omega(t)} \rho = 0, \tag{15}$$

$$\frac{d}{dt}\int_{\omega(t)} \rho\mathbf{u} = -\int_{\omega(t)} \nabla p_T, \tag{16}$$

$$\frac{d}{dt}\int_{\omega(t)} \rho E = -\int_{\omega(t)} \nabla \cdot p_T\mathbf{u}. \tag{17}$$

During this phase, the integration domain $\omega(t)$ moves this time at the speed of the fluid $\mathbf{u}$. Compared to the classical Euler equations, the total pressure $p_T = p + \frac{aT^4}{3}$ has substituted the matter pressure p and the total matter energy is increased by the internal radiative energy $E = e + \frac{\mathbf{u}^2}{2} + \tau a T^4$. It is shown that this new system is a hyperbolic system of conservation laws whose properties are identical to those of Euler's equations. A standard analysis (see for example [Bressan, 2000, Dafermos, 2000, Després, 2017] or [Godlewski and Raviart, 1995]) shows that, projected in one direction $\mathbf{n}$, the Jacobian matrix of this system admits three real eigenvalues $\lambda_1 = \mathbf{u}\cdot\mathbf{n} - c_T$, $\lambda_2 = \mathbf{u}\cdot\mathbf{n}$ and $\lambda_3 = \mathbf{u}\cdot\mathbf{n} + c_T$, with $c_T^2 = \frac{\partial p_T}{\partial \rho} = c^2 + \frac{4}{3}p_r\tau$, where $c^2 = \frac{\partial p(\rho,\eta_m)}{\partial \rho}$ is the square of the sound speed in the matter. As for the classical Euler equations, λ_1 and λ_3 correspond to truly non-linear fields (rarefaction or shock waves) while λ_2 corresponds to a linearly degenerate field (contact discontinuity). For this sub-system, the Clausius-Duhem inequality writes

$$\rho\frac{D}{Dt}\eta \geq 0, \tag{18}$$

and in integral form

$$\forall \omega(t) \subset \Omega(t), \frac{d}{dt}\int_{\omega(t)} \rho\eta \geq 0, \tag{19}$$

with equality only in the case of reversible processes, i.e. in the absence of shock.

With a few subtleties concerning the use of the equations of state, we are therefore in the (relatively) reassuring (because very well known) framework of the Euler system of equations. The chapter 1 of this manuscript is dedicated to my contributions to the development and the extension of schemes to solve these equations.

Phase II In this phase we solve the problem of non-linear diffusion on the fixed domain resulting from the previous resolution. $\forall \omega \subset \Omega$,

$$\begin{aligned}
\frac{d}{dt}\int_{\omega} 1 &= 0,\\
\frac{d}{dt}\int_{\omega} \rho &= 0,\\
\frac{d}{dt}\int_{\omega} \rho\mathbf{u} &= \mathbf{0},\\
\frac{d}{dt}\int_{\omega} \rho E &= \int_{\omega} \nabla \cdot k\nabla T^4.
\end{aligned}$$

The first three equations are a direct consequence of the fact that hydrodynamics is frozen. Only the last equation presents a difficulty.

Since the variation in kinetic energy is zero,

$$\forall \omega(t) \subset \Omega(t), \frac{d}{dt}\int_{\omega} \rho E = \frac{d}{dt}\int_{\omega} \left(\rho e(T) + aT^4\right).$$

We can therefore simplify our discussion by considering only the last equation in the form:

$$\frac{\partial}{\partial t}\left(\rho e(T) + aT^4\right) = \nabla \cdot k\nabla T^4. \tag{20}$$

In this equation, the radiative diffusion coefficient is calculated by

$$k = \frac{ac}{3\sigma},$$

where c is the speed of light and σ is the Rosseland opacity (see for instance [Mihalas and Weibel-Mihalas, 1999] p. 464). This opacity is a non-linear function of T (ρ being constant for frozen hydrodynamics). In this context, the specific internal energy e is also a non-linear function of T only. This problem can be equivalently formulated as an entropy evolution problem, in the form of

$$\rho\frac{\partial}{\partial t}\eta(T) = \nabla \cdot \frac{K}{T}\nabla T + \frac{K}{T^2}\nabla T \cdot \nabla T. \tag{21}$$

or

$$\forall \omega \subset \Omega, \quad \frac{d}{dt}\int_\omega \rho\eta = \int_\omega \nabla \cdot \frac{K}{T}\nabla T + \int_\omega \frac{K}{T^2}\nabla T \cdot \nabla T. \tag{22}$$

Physical considerations make it possible to choose an increasing function $X(T)$ which allows to minimize the non-linearities of the equivalent system (under the condition $\frac{de}{dT} > 0$)

$$\frac{\partial}{\partial t}X = \alpha(X)\nabla \cdot \beta(X)\nabla X. \tag{23}$$

This is a non-linear parabolic equation. The second part 2 of this manuscript is dedicated to my contributions to the development of a method to solve this equation.

Phase III In the last phase of the method, we want to change the integration space. From a continuous point of view, the solved equation is trivially

$$\frac{\partial \varphi}{\partial t} = 0, \quad \text{with } \varphi = \tau,\ \rho,\ \rho\mathbf{u} \text{ or } \rho E.$$

If we integrate these equations over a domain $\omega(t)$ moving at a speed of $\mathbf{w}$, using Reynolds transport theorem, we get, $\forall \omega(t) \subset \Omega(t)$

$$\frac{d}{dt}\int_{\omega(t)} 1 - \int_{\omega(t)} \nabla \cdot \mathbf{w} = 0, \tag{24}$$

$$\frac{d}{dt}\int_{\omega(t)} \rho - \int_{\omega(t)} \nabla \cdot \rho\mathbf{w} = 0, \tag{25}$$

$$\frac{d}{dt}\int_{\omega(t)} \rho\mathbf{u} - \int_{\omega(t)} \nabla \cdot \rho\mathbf{w} \otimes \mathbf{u} = \mathbf{0}, \tag{26}$$

$$\frac{d}{dt}\int_{\omega(t)} \rho E - \int_{\omega(t)} \nabla \cdot \rho\mathbf{w}E = 0. \tag{27}$$

Since the integration domain ω moved at the speed $\mathbf{u}$ during phase I, its overall speed corresponding to the sequence of phases I, II and III corresponds to $\mathbf{u}_a = \mathbf{u} + \mathbf{0} + \mathbf{w}$. This last phase is obviously isentropic, and the corresponding balance equation is written in the same way:

$$\forall \omega(t) \subset \Omega(t), \quad \frac{d}{dt}\int_{\omega(t)} \rho\eta - \int_{\omega(t)} \nabla \cdot \rho\eta\mathbf{w} = 0. \tag{28}$$

This third step seems artificial from the point of view of the continuous system, but it models the discretization we use. This phase leads naturally to the mixing of fluids in the case where several constituents are considered. This poses new numerical and modelling problems. The chapter 3 is dedicated to the numerical studies I have done concerning this phase.

It is easily verified that the sums of the fluxes of phases I, II and III are equal to the fluxes of the equations (1)-(4) and that the Clausius-Duhem inequality obtained by summation of (19), (22) and (28) is also identical to (6).

The work presented in the remainder of this manuscript is concerned with the resolution of these three phases, and thus these three systems of equations. The objective is to provide discretizations of the above-mentioned operators respecting the properties of conservation, consistency and stability associated with the Lax-Wendroff [Lax and Wendroff, 1960] theorem. For the stability, we try to ensure at the discrete level the properties recalled in page 2.

The work described in this manuscript also fits into an HPC (High Performance Computing) framework. All the algorithms proposed have therefore been parallelized by mesh partitioning. This implies that the control of data flows between the computing cores is a parameter to be taken into account in the efficiency of the schemes. Even if it is not the main object of this manuscript, it will be referred to when it has an impact on the construction of numerical methods.

Consistency *is the foundation of virtue*

Francis Bacon

1

Numerical methods for hydrodynamics

Contents

1.1 Introduction

In this chapter we seek to resolve Phase I described in the general introduction, i.e. the system (14-17) presented in page 3. The context recalled in the previous chapter - strongly compressible flow, mesh moving at the speed of the fluid - imposes us to use a scheme adapted to unstructured meshes and verifying the hypothesis of the Lax-Wendroff [Lax and Wendroff, 1960] theorem: consistency, conservation, entropic character. These constraints have been the guiding thread of the work presented in this section. Before listing my works, it is useful to make a quick inventory of available schemes for compressible hydrodynamics in Lagrangian reference frame (i.e. on mobile mesh at the fluid velocity). For more details on these methods, the reader can refer to the review articles [Barlow et al., 2016a, Benson, 1992c, Loubère et al., 2016].

The first discretization of the system of compressible Euler equations, the VNR (Von Neumann Richtmyer) scheme, is due to Von Neumann and Richtmyer [Neumann and Richtmyer, 1950b] in 1950. This mono-dimensional scheme is based on a staggered discretization of the unknowns. The thermodynamic unknowns (density, internal energy) are discretized at the cell centers, while the velocity is discretized at the vertices of the mesh. This founding work has been to the origin of numerous extensions and improvements for more than 60 years. Without seeking to be exhaustive, it should be noted that the problem of conservation of the scheme was corrected in 1D by Trulio and Trigger [Trulio and Trigger, 1961], and in 2D much later by Burton [Burton, 1990]. More recently,

a staggered in time and conservative version was formulated in [Llor et al., 2016]. The original scheme has been extended to 2D and elasticity by Wilkins [Wilkins, 1964b]. The 2D axi-symmetric conservative extension in total energy is described in [Caramana et al., 1998b]. A very high-order version of this scheme has recently been published [Dobrev et al., 2012], and reinterpreted in the context of residual distribution schemes [Abgrall and Tokareva, 2017]. This scheme is at the heart of many Lagrangian codes over the past 60 years. The main flaw of this method is that it is very difficult to extend it to an Arbitrary Lagrange Euler (ALE) scheme. This is why new Lagrangian methods based on an acoustic Godunov solver have been developed. These methods are based on a finite volume approach, where all unknowns are represented by their mean values on the mesh elements, which makes the extension to the ALE more natural. Fluxes are calculated by solving Riemann's problems at the boundaries of the cells according to Godunov's original idea [Godunov, 1959]. This type of scheme was originally designed for use in an Eulerian frame. They have been extended for the first time to the Lagrangian multi-D frame in the CAVEAT [Addessio et al., 1990] code. The fluxes were then computed at the edges of the 2D mesh, which posed the problem of mesh displacement. This difficulty was overcome by Després & Mazeran [Després and Mazeran, 2005, Mazeran, 2007b] who proposed a Riemann solver at the mesh vertices. Since this work, the interest in finite volume schemes for Lagrangian hydrodynamics has been considerable, and has resulted in numerous publications. The centred schemes have been developed in particular at the CELIA in Bordeaux (for example [Maire et al., 2007b, Maire, 2009b, 2011b, Georges et al., 2016]), at LANL at Los-Alamos (among others [Burton et al., 2013b, 2015a, Morgan et al., 2015]), as well as than at the BARC in India (for example [Sijoy and Chaturvedi, 2015, 2016]). At least two teams are working on this subject at IAPCM in China (for example [Li et al., 2014, Liu et al., 2015, Sun et al., 2016]). Other researchers are interested in it also (for example [Barlow and Roe, 2011, Barlow, 2013, Cheng and Shu, 2010, Corot and Mercier, 2018, Vilar et al., 2016a]). My colleagues of the CEA and I have also an important contribution to the development of these methods, from part detailed in the following, but see also [Braeunig, 2016, Braeunig and Chaudet, 2017, Paulin et al., 2019].

The work described in this section has been carried out within the framework of this strain of scheme. For the sake of simplicity, I adopt the formalism used in [Carré et al., 2009a]. However, the results presented apply to any scheme of this family (finite volume scheme with Riemann solver at vertices).

1.2 Structure of the finite volume schemes for the semi-Lagrangian

We're interested in the resolution of the system (14-17) presented in page 3. These equations are valid for any sub-domain moving at the speed of the fluid. We give ourselves a regular mesh $\mathcal{M}(t)$ of $\Omega(t)$. We consider here that $\mathcal{M}(t)$ is defined by a finite collection of cells j that partition $\Omega(t)$. Specifically, we have

$$
\begin{aligned}
&1.\forall j \in \mathcal{M}, \quad j \subset \Omega,\\
&2.\forall \mathbf{x} \in \Omega, \quad \exists j \in \mathcal{M} \text{ s. t. } \mathbf{x} \in \bar{j},\\
&3.\forall j,k \in \mathcal{M}, \quad \bar{j} \cap \bar{k} \neq \emptyset \Longleftrightarrow \left| \begin{array}{l} j = k, \\ \text{ or} \\ \partial j \cap \partial k \neq \emptyset \text{ and } j \cap k = \emptyset. \end{array} \right.
\end{aligned}
$$

The last relationship indicates that if two distinct cells intersect, it can only be through a piece of their edge (possibly a vertex). The equations (14-17) imply then that $\forall j \in \mathcal{M}$,

$$\frac{d}{dt}\int_j 1 = \int_j \nabla \cdot \mathbf{u} \tag{1.1}$$

$$\frac{d}{dt}\int_j \rho = 0, \tag{1.2}$$

$$\frac{d}{dt}\int_j \rho \mathbf{u} = -\int_j \nabla p_T \tag{1.3}$$

$$\frac{d}{dt}\int_j \rho E = -\int_j \nabla \cdot p_T \mathbf{u}. \tag{1.4}$$

To induce a finite volume structure, Green's formula is applied. Strictly speaking, this requires assumptions of regularity on ($\mathbf{u}$ and p_T) in the integration domain. We thus make the hypothesis (initially formulated by Godunov [Godunov, 1959]) that the discontinuities of these functions are located at the edges of each cell j of the mesh. Thanks to this very strong hypothesis, we can write that $\forall j \in \mathcal{M}$

$$\frac{d}{dt}\int_j 1 = \int_{\partial j} \mathbf{u}\cdot\mathbf{n}, \tag{1.5}$$

$$\frac{d}{dt}\int_j \rho = 0, \tag{1.6}$$

$$\frac{d}{dt}\int_j \rho\mathbf{u} = -\int_{\partial j} p_T\mathbf{n}, \tag{1.7}$$

$$\frac{d}{dt}\int_j \rho E = -\int_{\partial j} p_T\mathbf{u}\cdot\mathbf{n}. \tag{1.8}$$

The principle of spatial discretization of finite-volume schemes for the Lagrangian is to compute a consistent approximation of the fluxes $-\int_{\partial j} p_T\mathbf{n}$ and $-\int_{\partial j} p_T\mathbf{u}\cdot\mathbf{n}$ of the equations (1.7) and (1.8) from the previous system, which updates the momentum and total energy. Rather than solving explicitly (1.5), we impose that the cell j moves at an approximate fluid velocity, which induces the variation of the volume. The equation (1.6) is trivially respected considering that the mass of j is constant.

Moving each cell at the speed of the fluid is the key to the success of Lagrangian methods. This is reflected at the continuous level as follows: $\forall \mathbf{x}_m \in j$, material point of the mesh j, $\frac{d}{dt}\mathbf{x}_m = \mathbf{u}(\mathbf{x}_m)$. It induces conservation of the volume (1.5), by applying this formula to the edge of each cell j. At this point, we can already state one of the Lagrangian challenges: the displacement of the mesh by a formula approximating $\frac{d}{dt}\mathbf{x}_m = \mathbf{u}(\mathbf{x}_m)$, must remain consistent with a discrete form of (1.5). This property is called GCL (for *Geometric Conservation Law*) [Farhat et al., 2001, Thomas and Lombard, 1979] and is an essential ingredient in building an effective Lagrangian scheme.

1.3 Spatial discretization

In the following, we adopt the classical convention in finite volumes

$$\varphi_j = \frac{1}{V_j}\int_j \varphi,$$

where $V_j = \int_j 1$ is the volume of the cell. In order not to make the notations more cumbersome, we note also

$$p_j = \frac{1}{V_j}\int_j p_T.$$

We explain in an abstract way in [Carré et al., 2009a], the principle of fabrication of Lagrangian finite volume schemes. As pointed out just before, an important component of the scheme is how to move the mesh, and the first step is to define the cell geometry according to a finite number of control points $(\mathbf{x}_r)_{1\leq r\leq N}$.

$$j = j(\mathbf{x}_1, \ldots, \mathbf{x}_N).$$

The essential idea is that this definition is not dependent on time, but only on the position of the control points. To fix the ideas, the simplest example is to assume that the cells are polygonal (or polyhedral) and entirely defined by the position of their vertices. However, this methodology extends to other types of cells (curved edges, non-conforming meshes,...) and will be one of the ingredients for the extension of these schemes (particularly detailed in the Sections 1.8 and 3.5).

It follows that the volume V_j of a mesh is also only a function of these control points

$$V_j = V_j(\mathbf{x}_1, \ldots, \mathbf{x}_N).$$

Using the chain rule, the variation in its volume is related to the variation in the positions of the control points by

$$\begin{aligned} V_j'(t) &= \sum_{r=1}^{N} \nabla_{\mathbf{x}_r} V_j \cdot \frac{d}{dt}\mathbf{x}_r, \\ &= \sum_{r\in\mathcal{R}_j} \nabla_{\mathbf{x}_r} V_j \cdot \mathbf{u}_r. \end{aligned}$$

In this expression, we noted $\mathcal{R}_j$, the set of control points defining the geometry of the cell j and $\mathbf{u}_r := \frac{d}{dt}\mathbf{x}_r$ the instantaneous velocity of the control point r. In doing so, it was assumed that the geometric definition of the cell did not change. For example, a polygonal cell defined by the position of its vertices is transformed into a polygonal cell of the same nature during its Lagrangian displacement, which is a second-order approximation in space.

By defining $\mathbf{C}_{jr} := \nabla_{\mathbf{x}_r} V_j$, one can rewrite the volume change as

$$V_j'(t) = \sum_{r\in\mathcal{R}_j} \mathbf{C}_{jr} \cdot \mathbf{u}_r. \tag{1.9}$$

We find in [Carré et al., 2009a] demonstrations of the properties of these vectors $\mathbf{C}_{jr}$ in plane geometry. I simply remind here the most useful ones for this presentation

$$V_j'(t) = \sum_{r\in\mathcal{R}_j} \mathbf{C}_{jr} \cdot \mathbf{u}_r, \tag{1.9}$$

$$V_j = \frac{1}{d} \sum_{r\in\mathcal{R}_j} \mathbf{C}_{jr} \cdot \mathbf{x}_r, \tag{1.10}$$

$$\sum_{r\in\mathcal{R}_j} \mathbf{C}_{jr} = \mathbf{0}, \tag{1.11}$$

$$\sum_{j\in\mathcal{J}_r} \mathbf{C}_{jr} = \mathbf{0}. \tag{1.12}$$

where $\mathcal{J}_r$ accounts for the set of cells sharing the vertex r. The relation (1.11) is relative to the invariance by translation of the volume, and is thus only verified in a Galilean frame. The last relation (1.12) is directly deduced from the conservation law of the volume. We can geometrically interpret these vectors $\mathbf{C}_{jr}$. In dimension 2, and for polygonal meshes, and if we suppose that the vertices of the cell j are ordered in trigonometric order, we have

$$\mathbf{C}_{jr} = -\frac{1}{2}(\mathbf{x}_{r+1} - \mathbf{x}_r)^\perp - \frac{1}{2}(\mathbf{x}_r - \mathbf{x}_{r-1})^\perp,$$

For the definition of the Eucclhyd scheme, it's useful to split the $\mathbf{C}_{jr}$ vector into $\mathbf{N}_{jr}^+ = -\frac{1}{2}(\mathbf{x}_{r+1}\mathbf{x}_r)^\perp$ and $\mathbf{N}_{jr}^- = -\frac{1}{2}(\mathbf{x}_r - \mathbf{x}_{r-1})^\perp$. We obviously have

$$\mathbf{C}_{jr} = \mathbf{N}_{jr}^+ + \mathbf{N}_{jr}^-.$$

The different notations are shown on the figure 1.1.

Since (1.9) is a discretization of the GCL, we have established

$$\sum_{r\in\mathcal{R}_j} \mathbf{C}_{jr} \cdot \mathbf{u}_r \approx \int_{\partial j} \mathbf{u}\cdot\mathbf{n} \left(= \int_j \nabla\cdot\mathbf{u}\right).$$

Specifically, $\sum_{r\in\mathcal{R}_j} \mathbf{C}_{jr} \cdot \mathbf{u}_r$ is the trapezoidal approximation of $\int_{\partial j} \mathbf{u}\cdot\mathbf{n}$. In all generality, we write for a vector function $\mathbf{f}$

$$\int_{\partial j} \mathbf{f}\cdot\mathbf{n} \approx \sum_{r\in\mathcal{R}_j} \mathbf{C}_{jr} \cdot \mathbf{f}(\mathbf{x}_r).$$

This approximation is second-order accurate, since the formula is exact (by construction) for continuous and affine functions on the edges of the cell j. Moreover, it does not depend on the dimension

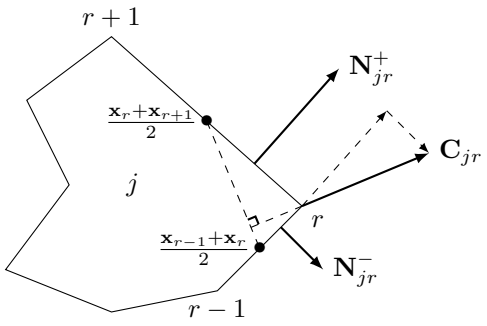

Figure 1.1: We represent the $\mathbf{C}_{jr}$ vector and the associated $\mathbf{N}_{jr}^{\pm}$ normals.

of the problem (1D, 2D or 3D), and does not prejudge the formula for the calculation of the volume. The only requirement is that it is analytically expressed as a function of the position of the vertices of the cell. This formalism has allowed us to extend this scheme in 3D [Carré et al., 2009a], as well as to non-conformities (Section 1.8) and to the sliding (Section 3.5).

The following approximation for the total energy balance is then deduced

$$-\int_j \nabla \cdot p\mathbf{u} \approx -\sum_{r\in\mathcal{R}_j} \mathbf{C}_{jr} \cdot (p\mathbf{u})_r.$$

The gradient operator is deduced from the divergence operator by a discrete duality argument. For the average pressure gradient this translates into

$$\int_j \nabla p \approx \sum_{r\in\mathcal{R}_j} \mathbf{C}_{jr} p_{jr}.$$

The semi-discrete scheme in space is therefore written as follows

$$\begin{aligned} V_j'(t) &= \sum_{r\in\mathcal{R}_j} \mathbf{C}_{jr} \cdot \mathbf{u}_r, \\ M_j'(t) &= 0, \\ M_j \mathbf{u}_j'(t) &= -\sum_{r\in\mathcal{R}_j} \mathbf{C}_{jr} p_{jr}, \\ M_j E_j'(t) &= -\sum_{r\in\mathcal{R}_j} \mathbf{C}_{jr} \cdot (p\mathbf{u})_{jr}. \end{aligned} \tag{1.13}$$

The finalization of the spatial discretization requires to determine the quantities $\mathbf{u}_r$, p_{jr} and $(p\mathbf{u})_{jr}$ according to the unknowns defined at the cells (ρ_j, $\mathbf{u}_j$, $\mathbf{E}_j$, $p_j, \ldots$). As for the acoustic Godunov solver, the total energy fluxes are deduced by imposing $(p\mathbf{u})_{jr} := p_{jr}\mathbf{u}_r$.

An essential ingredient of this scheme is that unlike classical multidimensional finite volume methods, flows are not computed at the faces of the cells, but at the vertices. This is a direct consequence of the construction of the divergence operator from the volume definition, and thus of the respect of the semi-discrete GCL. The fact that the nodal pressure p_{jr} depends on the cell, and thus can be potentially discontinuous at the vertex, is another originality of the scheme which is explained in the following.

These two ideas were formulated by Després and Mazeran in [Després and Mazeran, 2003, Després and Mazeran, 2005], and repeated in the construction of all Lagrangian finite-volume schemes since then. The property of entropy growth verified by these schemes derives from this.

It now remains to be determined $\mathbf{u}_r$ and p_{jr}. It is empirically observed that the Godunov acoustic scheme gives excellent results in Lagrangian [1]. It is therefore decided to mimic its construction and

[1] while its equivalent in the Eulerian frame is not satisfactory.

to impose in a certain direction $\mathbf{n}$, the acoustic Riemann invariant

$$dp + \rho c d\mathbf{u} \cdot \mathbf{n} = 0,$$

to relate the constant states $(\mathbf{u}_j, p_j)$ of a grid cell to the nodal quantities $(\mathbf{u}_r, p_{jr})$. So we write in any vertex r a discrete expression of this invariant

$$\forall j \in \mathcal{J}_r, \quad p_{jr} - p_j + (\rho c)_j (\mathbf{u}_r - \mathbf{u}_j) \cdot \mathbf{n}_{jr} = 0, \tag{1.14}$$

where $\mathbf{n}_{jr}$ designates a direction. Choosing a cell dependent nodal pressure p_{jr} implies that the number of nodal unknowns is d (for velocity $\mathbf{u}_r$) + $\#\mathcal{J}_r$ (for pressure p_{jr}) and the number of equations is $\#\mathcal{J}_r$. The additional d equations necessary to be able to determine $(\mathbf{u}_r, (p_{jr})_{j\in\mathcal{J}_r})$ uniquely are induced by the constraint of conservation of the momentum of the system (1.13). Thus, one imposes [2]

$$\sum_{j\in\mathcal{J}_r} \mathbf{C}_{jr} p_{jr} = \mathbf{0}. \tag{1.15}$$

This construction explains the need to make the nodal pressure depend on the cell.

For the problem (1.14)–(1.15) to be well posed, it is sufficient that $\mathbf{u}_r$ be uniquely defined. By injecting the equations (1.14) into (1.15), after some elementary calculations, we obtain

$$\sum_{j\in\mathcal{J}_r} A_{jr}\ \mathbf{u}_r = \sum_{j\in\mathcal{J}_r} A_{jr}\mathbf{u}_j + \sum_{j\in\mathcal{J}_r} \mathbf{C}_{jr} p_j, \qquad \text{with} \quad A_{jr} := (\rho c)_j \mathbf{C}_{jr} \otimes \mathbf{n}_{jr}.$$

If the matrix $A_r := \sum_{j\in\mathcal{J}_r} A_{jr}$ is non-singular, then $\mathbf{u}_r$ is unique. The Glace scheme consists in choosing

$$\mathbf{n}_{jr} := \frac{\mathbf{C}_{jr}}{\|\mathbf{C}_{jr}\|}. \tag{1.16}$$

In this case, the matrices A_{jr} are non-negative symmetric and of rank 1. A_r is therefore a non-negative symmetric matrix. For it to be in addition of rank d and thus non-singular, it is sufficient that the family $\{\mathbf{C}_{jr}\}_{j\in\mathcal{J}_r}$ is a generator of $\mathbb{R}^d$. This is the case for any internal vertex of an "admissible" mesh.

From this matrix formulation, it is possible to write most of the finite-volume schemes for the Lagrangian, cited in the introduction to this chapter. For this it is necessary to rewrite Riemann's solver (1.14) in vector form, like [Kluth and Després, 2010, Kluth, 2008] and [Maire, 2011b]. The general structure (1.17)–(1.22) is as follows

$$V_j'(t) = \sum_{r\in\mathcal{R}_j} \mathbf{C}_{jr} \cdot \mathbf{u}_r \tag{1.17}$$

$$M_j'(t) = 0, \tag{1.18}$$

$$M_j \mathbf{u}_j'(t) = -\sum_{r\in\mathcal{R}_j} \mathbf{F}_{jr}, \tag{1.19}$$

$$M_j E_j'(t) = -\sum_{r\in\mathcal{R}_j} \mathbf{F}_{jr} \cdot \mathbf{u}_r, \tag{1.20}$$

where $\mathbf{F}_{jr}$ and $\mathbf{u}_r$ are given by

$$\mathbf{F}_{jr} := A_{jr}(\mathbf{u}_j - \mathbf{u}_r) + \mathbf{C}_{jr} p_j, \tag{1.21}$$

$$\sum_{j\in\mathcal{J}_r} \mathbf{F}_{jr} = \mathbf{0}. \tag{1.22}$$

[2] In the case $d = 1$, $\mathbf{C}_{jr}$ is worth -1 for the left vertex of the cell j and 1 for the right vertex. So if j_- and j_+ designate the cells to the left and right of the vertex r, (1.15) is written $p_{j_-} - p_{j_+} = 0$. We then have only one pressure at the vertex and we find the Godunov acoustic solver.

This structure is common to Lagrangian finite-volume schemes with a nodal Riemann solver. We find for example, Glace [Després and Mazeran, 2005], Eucclhyd [Maire et al., 2007b] and CCH [Burton et al., 2013b] with the following choice of matrices A_{jr}

$$\begin{aligned}
\text{Glace}: \quad & A_{jr} := (\rho c)_j \frac{\mathbf{C}_{jr} \otimes \mathbf{C}_{jr}}{\|\mathbf{C}_{jr}\|}, \\
\text{Eucclhyd}: \quad & A_{jr} := (\rho c)_j \left(\frac{\mathbf{N}^+_{jr} \otimes \mathbf{N}^+_{jr}}{\|\mathbf{N}^+_{jr}\|} + \frac{\mathbf{N}^-_{jr} \otimes \mathbf{N}^-_{jr}}{\|\mathbf{N}^-_{jr}\|} \right), \\
\text{CCH}: \quad & A_{jr} := (\rho c)_j \left(\mathbf{N}^+_{jr} + \mathbf{N}^-_{jr} \right) \cdot \mathbf{a}_j I_d,
\end{aligned}$$

where I_d is the identity matrix of $\mathbb{R}^d \times \mathbb{R}^d$ and $\mathbf{a}_j$ is the direction of acceleration in the cell j. This is the structure that is used afterwards.

1.4 Properties of semi-discrete schemes

In this section, I recall the properties of the schemes defined by (1.17)–(1.22) in the case where A_{jr} is non-negative symmetric and $A_r := \sum_{j \in \mathcal{J}_r} A_{jr}$ is non-singular. These properties are: **volume, mass, momentum, and total energy conservation, entropy growth, and consistency**. These are the hypotheses of the Lax-Wendroff Theorem [Lax and Wendroff, 1960].

Conservation Centered schemes having the structure of nodal solvers (1.17)–(1.22) are conservative in volume, mass, momentum and total energy. These properties are only due to the flux formulation and are therefore independent of a possible reconstruction of $\mathbf{u}_j$ and p_j for high-order extensions. They remain true also for explicit time integration. The demonstration of this property is simple and can be found for example in [Després and Mazeran, 2005].

Entropy behaviour Now let us look at the stability of centered schemes. To do this, we check the evolution of their entropy. We obviously consider the case of a first-order schema in space: $\mathbf{u}_j$ and p_j are constant per cell. The demonstration of this property can also be found in [Després and Mazeran, 2005]. I reproduce it here, however, because some elements are used in the remainder of the manuscript.

According to the second principle of thermodynamics, η grows for physical solutions. Gibbs' formula says $Td\eta = pd\tau + de$, which is translated into $T_j \frac{d}{dt}\eta_j = p_j \frac{d}{dt}\tau_j + \frac{d}{dt}e_j$. We trivially have

$$M_j T_j \frac{d}{dt}\eta_j = M_j p_j \frac{d}{dt}\tau_j + M_j \frac{d}{dt}e_j.$$

Since $V_j = M_j \tau_j$ et $e_j = E_j - \frac{1}{2}\mathbf{u}_j \cdot \mathbf{u}_j$, one obtains

$$M_j T_j \frac{d}{dt}\eta_j = p_j \frac{d}{dt}V_j \ + \ M_j \frac{d}{dt}E_j \ - \ \mathbf{u}_j \cdot M_j \frac{d}{dt}\mathbf{u}_j.$$

Using (1.17)–(1.20), one gets

$$M_j T_j \frac{d}{dt}\eta_j = p_j \sum_{r \in \mathcal{R}_j} \mathbf{C}_{jr} \cdot \mathbf{u}_r \ - \ \sum_{r \in \mathcal{R}_j} \mathbf{F}_{jr} \cdot \mathbf{u}_r \ + \ \mathbf{u}_j \cdot \sum_{r \in \mathcal{R}_j} \mathbf{F}_{jr}.$$

By definition $\mathbf{F}_{jr} = A_{jr}(\mathbf{u}_j - \mathbf{u}_r) + \mathbf{C}_{jr} p_j$, then after elementary calculations, one finds

$$M_j T_j \frac{d}{dt}\eta_j = \sum_{r \in \mathcal{R}_j} (\mathbf{u}_j - \mathbf{u}_r)^T A_{jr} (\mathbf{u}_j - \mathbf{u}_r). \tag{1.23}$$

Since by construction the matrices A_{jr} are positive, $M_j T_j \frac{d}{dt}\eta_j \geq 0$, and since M_j and T_j are positive, we have $\frac{d}{dt}\eta_j \geq 0$.

Consistency We do not give in this presentation the demonstration of the consistency of the centered schemes, this proof being quite technical. Let us underline nevertheless that Després demonstrated it in [Després, 2010c] for the Glace scheme and that this demonstration extends without difficulty to the Eucclhyd scheme.

Galilean invariance Euler's equations are invariant by a change of Galilean frame (see [Godlewski and Raviart, 1995] for example). If we use an Eulerian scheme (*i.e.* the grid is motionless from one time step to another), this property is generally lost. At convergence, however, it can be restored.

On the other hand, Lagrangian schemes generally preserve this property. Centered schemes are invariant by changing the Galilean reference frame. It is sufficient to consider (1.21) to be convinced. The same is true for indirect ALE methods (as considered in this manuscript) as soon as the grid is regularized by positions differences.

1.5 Time integration

At first-order, an explicit Euler scheme is used to integrate the time derivative. All quantities are known at time t^n, we can then compute the **explicit** fluxes $\mathbf{u}_r^n$ and $\mathbf{F}_{jr}^n$, by solving in each vertex

$$\left| \begin{array}{l} \forall j \in \mathcal{J}_r, \quad \mathbf{F}_{jr}^n = A_{jr}^n(\mathbf{u}_j^n - \mathbf{u}_r^n) + \mathbf{C}_{jr}^n p_j^n, \\ \qquad \displaystyle\sum_{j \in \mathcal{J}_r} \mathbf{F}_{jr}^n = \mathbf{0}. \end{array} \right.$$

Having determined a time step δt^n, we can update the data to time $t^{n+1} = t^n + \delta t^n$. The coordinates of the vertices of the mesh are then given by $\mathbf{x}_r^{n+1} := \mathbf{x}_r^n + \delta t^n \mathbf{u}_r^n$. We can then calculate the vectors $\mathbf{C}_{jr}^{n+1}$ according to the new $\mathbf{x}_r^{n+1}$ and the new volumes of the cells $V_j^{n+1} := \frac{1}{d}\sum_{r\in\mathcal{R}_j} \mathbf{C}_{jr}^{n+1} \cdot \mathbf{x}_r^{n+1}$. As the masses of the cells are constant, we obtain the density $\rho_j^{n+1} := \frac{M_j}{V_j^{n+1}}$. The new velocities and total energies are obtained by

$$\mathbf{u}_j^{n+1} := \mathbf{u}_j^n - \frac{\delta t^n}{M_j} \sum_{r\in\mathcal{R}_j} \mathbf{F}_{jr}^n,$$

$$\text{and} \quad E_j^{n+1} := E_j^n - \frac{\delta t^n}{M_j} \sum_{r\in\mathcal{R}_j} \mathbf{F}_{jr}^n \cdot \mathbf{u}_r^n.$$

We can then calculate the internal energy in each cell $e_j^{n+1} := E_j^{n+1} - \frac{1}{2}\|\mathbf{u}_j^{n+1}\|^2$. We thus obtain the new pressure $p_j^{n+1} := p(\rho_j^{n+1}, e_j^{n+1})$ and the new speed of sound $c_j^{n+1} := c(\rho_j^{n+1}, e_j^{n+1})$, necessary for the calculation of A_{jr}^{n+1}.

Properties of the fully discrete scheme The properties of conservation and consistency of the semi-discrete scheme are preserved by the time integration. On the other hand, the stability condition must be discussed again. In the introduction, the objectives regarding stability have been displayed. In this (hydrodynamic) phase, the aim is to ensure the positivity of ρ and T at the discrete level, as well as the growth of entropy. While it is possible to exhibit time step constraints that ensure that the density remains positive and that the energy admits a lower bound (and therefore the temperature is positive), the case of the entropy production is more tricky. Indeed, the only results published are results of the existence of a strictly positive time step δt ensuring growth of entropy (see by example [Després, 2001, Gallice, 2003]).

As a consequence, there is not (yet) a reliable method of prediction *a priori* of δt. In practice, we use formula of the kind

$$\forall j, \quad c_j \frac{\delta t}{\delta x_j} < \text{CFL},$$

with δx_j a characteristic local length defined as the ratio of the volume to the surface of the cell j. This condition is generally sufficient to ensure the growth of entropy. However, a *a posteriori*

check of entropy growth is performed [Hoch and Labourasse, 2014, Del Pino et al., 2020a]. This can lead to a reduction the time-step of the incriminated iteration. This procedure is also discussed in Section 1.6.2.

1.6 Second-order extension

in collaboration with G. Carré, S. Del Pino, B. Després, P. Hoch

As we have just seen from a theoretical point of view, centered schemes are very good candidates for the simulation of gas dynamics in Lagrangian coordinates. Nevertheless, like all finite volume methods, these schemes are by construction first-order accurate. It is empirically observed that, even for very compressible applications and in the presence of strong shocks, the extension to the second-order brings a considerable gain in terms of accuracy at fixed computation time. Moreover, it makes it possible to respond (at least partially) to one of the main objections to this type of scheme, which is the non-respect of isentropic solutions. The growth of entropy for regular solutions is considerably reduced by the extension to order 2 (cancelled for affine solutions).

In addition, we naturally benefit from the rich experience of high-order extension for finite volume schemes (see for example [Godlewski and Raviart, 1995, Leveque, 2002, Toro, 1997]).

We published the first second-order extension for the centered schemes in [Carré et al., 2009a]. It uses the principles of the MUSCL approach for the order in space extension [van Leer, 1979], and Runge-Kutta for the order in time extension. It has been improved by Maire [Maire, 2009c, 2011b], which is based on solving a generalized Riemann problem and a least-squares reconstruction of gradients. Our work on flux limiters has enabled us to make the second-order scheme invariant by changing the Galilean reference frame [Hoch and Labourasse, 2014]. Finally, the limitation *a posteriori* [Hoch and Labourasse, 2014, Del Pino et al., 2020a] that we propose, ensures that the high-order scheme meets the stability conditions ($\rho >0$, $T >0$, $dS >0$). In the following I describe the ingredients of the order extension in space we've been working on. The order extension in time is performed using Runge-Kutta or Strong-Stability-Preserving [Gottlieb et al., 2001] Runge-Kutta methods (an alternative high-order extension based on Generalised Riemann Solvers is proposed in [Maire, 2011b]). It does not rise any particular difficulties, and will not be addressed.

1.6.1 Second-order fluxes

The MUSCL method consists in reconstructing an affine function $\bar{\varphi}_j(\mathbf{x})$ in each cell from the mean values $\{\varphi_i\}_{i\in\mathcal{J}(j)}$ in this cell and its neighbors. For this, we calculate an approximate gradient $\mathbf{g}_j$ constant per cell by a least squares method. We then have an affine approximation of φ accurate to the second-order

$$\bar{\varphi}(\mathbf{x}) := \varphi_j + \mathbf{g}_j \cdot (\mathbf{x} - \mathbf{x}_j).$$

where $\mathbf{x}_j$ is the mass center of the cell j. By construction $\bar{\varphi}(\mathbf{x})$ verifies $\int_j \bar{f}_j = V_j f_j$.

This procedure is applied to unknowns $\mathbf{u}_j$ and p_j. Finally, the reconstructed values of these unknowns are substituted to the mean values in the Riemann solver (1.17)–(1.22)

$$\mathbf{F}_{jr} := A_{jr}(\bar{\mathbf{u}}_j(\mathbf{x}_r) - \mathbf{u}_r) + \mathbf{C}_{jr}\bar{p}_j(\mathbf{x}_r).$$

We then get exact fluxes for affine $\mathbf{u}$ and p functions.

1.6.2 Limitation

Godunov's theorem [Godunov, 1954] shows that in their version of order 2, centered schemes cannot guarantee the preservation of the admissible domain of solutions. In other words, the positivity of density and temperature, and the entropy growth are not assured.

The limitation generically consists in substituting $\bar{\varphi}_j(\mathbf{x})$ by

$$\bar{\varphi}_j^L(\mathbf{x}) := \varphi_j + \alpha_j \left(\bar{\varphi}_j(\mathbf{x}) - \varphi_j\right), \quad \text{with } \alpha_j \in [0, 1[, \tag{1.24}$$

in areas where the solution is not regular. There are many procedures to calculate α_j in the literature. In practice we use Minmod [Toro, 1997] or Barth-Jespersen [Barth and Jespersen, 1989b]. This wide

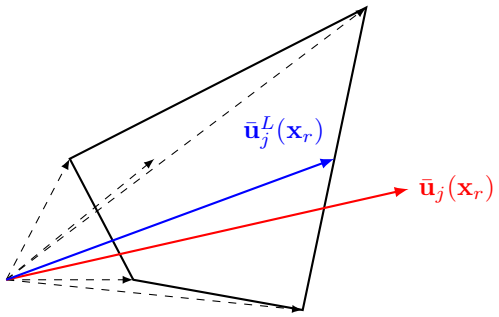

Figure 1.2: **Principle** : the quadrilateral represents the convex hull defined by the velocities of the cell j and of a neighborhood (dotted line). • $\bar{\mathbf{u}}_j(\mathbf{x}_r)$ is the reconstructed velocity. • $\bar{\mathbf{u}}_j^L(\mathbf{x}_r)$ its limited counterpart is into the convex hull.

range of limiters available is symptomatic of the fact that the problem of limitation is open. Recent studies (see for example [Berthon and Desveaux, 2014]), show in fact that, even in dimension 1, no existing *a priori* limiter can systematically guarantee the growth of entropy. This problem is the source of many recent publications (see for example [Perthame and Shu, 1996, Zhang and Shu, 2010, Cheng and Shu, 2014a, Guermond et al., 2018]). We show that this property can be restored using the limiters *a posteriori* [Hoch and Labourasse, 2014, Del Pino et al., 2020a] presented in Subsection 1.6.2. Another pitfall is related to the fact that the limiters available in the literature apply to scalar fields. Indeed, in contrast to the order extension, limitation is a highly non-linear process. It follows that applying it to vectors or tensors component by component makes the scheme lose the Galilean invariance property recalled in Section 1.4. We explain in the next subsection how we have addressed this problem.

Vector limitation

As we have just seen, if the reconstruction is a linear step in the order extension, the limitation phase is non-linear. This non-linearity induces that limiting vector (or tensor) quantities as a collection of independent scalars (component by component, $\bar{\mathbf{u}}_j(\mathbf{x}) := (\bar{u}_j^x(\mathbf{x}), \bar{u}_j^y(\mathbf{x}))$) does not preserve the discrete Galilean invariance. This has particularly significant effects on the preservation of the symmetries of the flows.

It is therefore necessary to use a vectorial approach for the limitation phase which generalizes the scalar case.

G. Luttwak and J. Falcovitz have recently proposed a limitation method for vector reconstructions [Luttwak and Falcovitz, 2011a] allowing to keep the Galilean invariance and thus the symmetries. This method named VIP (*Vector Image Polygon*) is a generalization to vectors of the classical ideas of limitations for scalar quantities.

The VIP method consists in replacing the notion of an admissible interval for scalar quantities by an admissible convex for vector quantities. The convex is defined by the convex hull induced by the vectors of the cell and its neighbours.

It is possible to define different variants of VIP which degenerate on the classical scalar limiters when the flow is one-dimensional and aligned with the mesh.

We show in [Hoch and Labourasse, 2014] how we adapted this method to centered schemes. In particular, we have chosen to construct convex hulls at each vertex of the mesh which allows to limit numerical dissipation as in [Burton et al., 2015a].

A posteriori Limitation

in collaboration with Ph. Hoch

The principle of the "APITALI" method (for *A Priori ITerAtive LImiter*) is based on simple numerical engineering considerations, and can be stated as follows: let us consider a A scheme with f_A fluxes satisfying the property set $\mathcal{P}_1$, and a B scheme with f_B fluxes satisfying the property set $\mathcal{P}_2$. Let us assume that conservation and consistency (in the flux sense) are properties of $\mathcal{P}_1$ and $\mathcal{P}_2$. So we can build a new flux $f_c = \beta f_a + (1-\beta) f_b$, which is also conservative and consistent. A judicious choice of β can then allow to benefit from all properties (ideally) $\mathcal{P}_1$ and $\mathcal{P}_2$. In the original

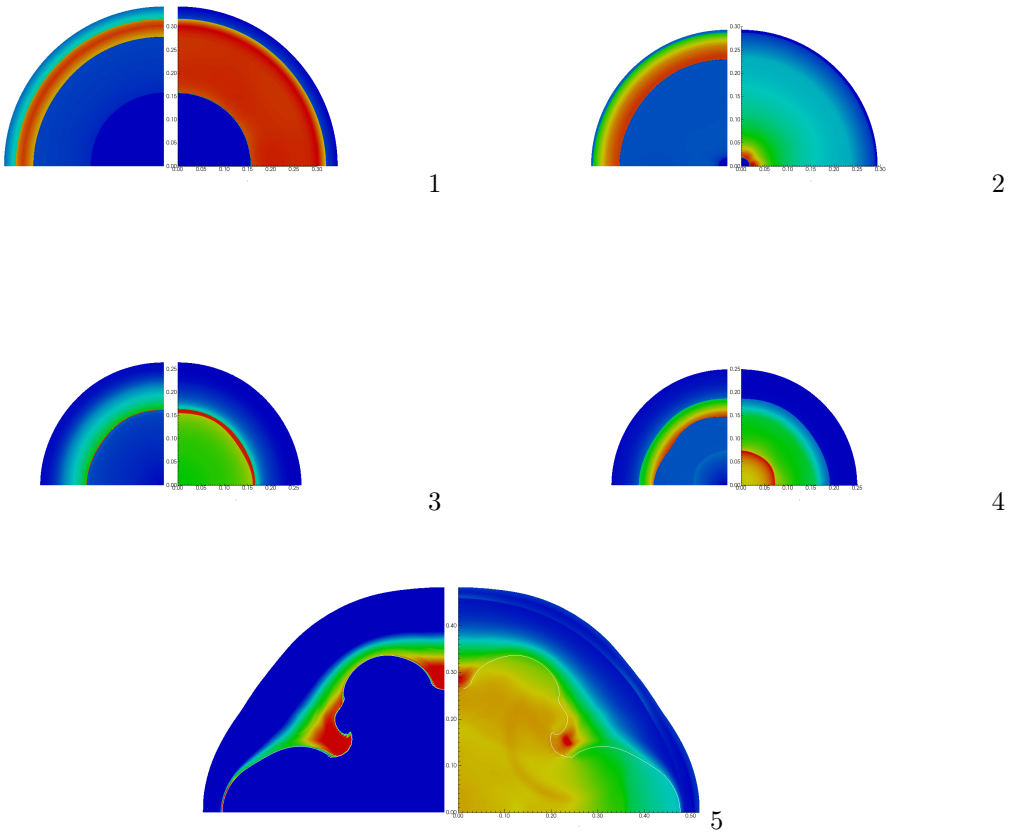

Figure 1.3: 2D-axisymmetric calculation of the collapse of a spherical shell disturbed by a Legendre 6 mode on a low density cavity. The Apitali method, thanks to the preservation of the rotational invariance, allows to compute the linear phase (Richtmyer-Meshkov instability, convergent, first three figures), and non-linear phase (Rayleigh-Taylor instability, divergent, last two figures) in a robust way. The left side of the figures represent density, and the one on the right represents pressure.

form introduced by P. Hoch in [Hoch, 2009], this principle is applied to finite volume schemes and to a MUSCL-type order extension such as the one used here. A is the 1st-order version and B is the 2nd-order version of the same scheme. The coefficient β_j then multiplies (or substitutes itself) to the coefficient α_j of the expression (1.24)

$$\bar{\varphi}_j^L(\mathbf{x}) := \varphi_j + \beta_j \alpha_j \left(\bar{\varphi}_j(\mathbf{x}) - \varphi_j\right), \quad \text{with } \alpha_j,\ \beta_j \in [0,1].$$

As suggested by the suffix of β_j, the evaluation of the coefficient is done locally. The schemes A and B are indeed conservative and consistent (in the sense of flux). According to whether one places oneself within the framework of the Lagrangian solver or of the projection, the property of the A scheme (of order 1) that one wants to preserve is either the growth of entropy or the principle of maximum. Indeed, the limiters presented in Section 1.6.2 are empirical attempts to restore to order 2 the above-mentioned properties, and may be insufficient to achieve this, even in 1D [Berthon and Desveaux, 2014]. It follows that it is an illusion to claim predict the value of β_j. So the process is iterative. It consists in performing a first calculation with $\beta_j = 1$ in all the cells, then decreasing β_j locally, at the locations where the property is violated, until the desired property is satisfied. This verification takes place *a posteriori*. This method naturally degenerates on the MOOD [Clain et al., 2011] method if β_j is set to zero as soon as the first iteration.

Several major advances for multi-dimensional numerical schemes are based on this simple approach.

For example, advection schemes respecting the Galilean invariance and the principle of maximum have been obtained [Hoch and Labourasse, 2014] by combining this approach with the notion of convex hull. The preservation of Galilean invariance induces invariance by rotation, and is, among other things, essential for the correct calculation of hydrodynamic instabilities of spherical shells.

It also provided Lagrangian schemes, both entropic and high-order accurate [Hoch and Labourasse, 2014, Del Pino et al., 2020a].

Finally, an extension to tensors, still based on the notion of convex hull, was also the subject of a Master 2 [Hervé, 2016] internship. This paves the way for limiters adapted to the Reynolds stress models for turbulence, or elasto-plasticity.

1.7 Subzone entropy stabilization

in collaboration with B. Després

Subzone entropy is a technique developed to improve the stability of centered schemes, mainly in Lagrangian frame. It should be stressed that this procedure is not intended to substitute for remeshing, in the case of mesh deformations induced by flow physics (shear, vortex,...). Its objective is to increase the robustness of the centered schemes in areas for which the use of the the above-mentioned remeshing techniques are inoperative or inappropriate — velocity or pressure boundary conditions, material interfaces that one wishes to keep Lagrangian (refer for example to the Section 3.5) — in order to complete the calculations.

This robustness problem can be interpreted as follows. Gibbs' law ensures that $Td\eta = de + pd\tau$. So, when the specific volume decreases, this has a negative contribution on the entropy balance. This contribution is necessarily compensated by an increase in internal energy to ensure the growth of entropy. This effect is reproduced algorithmically by the Glace and Eucclhyd scheme solver (see Section 1.4). Unfortunately, this property is not sufficient to prevent mesh degeneration (cell tangling), except in the particular case where the cells are simplex (one quadrangular cell can tangle while algebraically increasing its volume, as opposed to a triangle). However, the properties of the scheme listed in Section 1.4 are no longer guaranteed in this case.

The problem of stabilizing Lagrangian schemes also arises in the context of staggered schemes and has given rise to an abundant literature. Two main concepts emerge from this work. The first consists in assimilating each cell to a solid and prohibiting certain zero energy deformations, which are considered parasitic [Flanaghan and Belytshko, 1982b, Caramana and Shashkov, 1998a]. This technique is called *hourglass control*. The second authorizes the modification of the velocity of the mesh vertices to avoid mesh tangling and is known as *untangling* [Freitag and Plassman, 2000b, Vachal et al., 2003a].

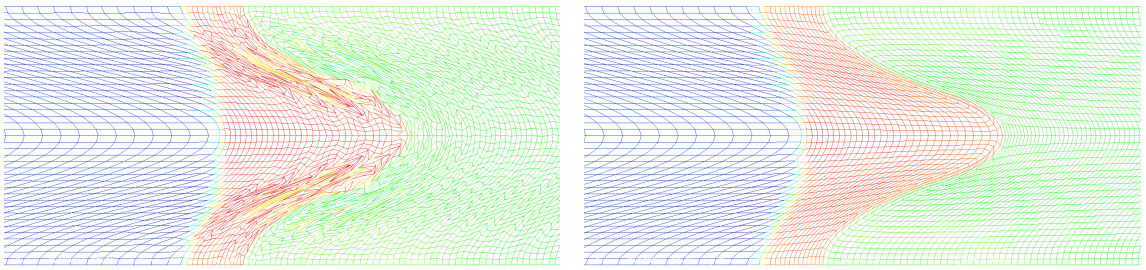

Figure 1.4: The use of subzone entropy (left), allows to correct the robustness problems of the Lagrangian calculus (right), while keeping the Lagrangian nature.

The approach developed within the framework of the centred schemes is based on other arguments. The idea is to transpose the good behaviour of the simplex to other types of elements. A preliminary and natural idea, consists in cutting the meshes into simplex. For relevant cuttings, the degeneration of any polygonal cell then corresponds to a triangle of zero or negative volume. A new entropy is constructed using the entropies from each of the sub-zone, by analogy with perfect gases,

$$\overline{\eta} := \eta + \gamma C_v \frac{\sum_i \log(4f^i)}{4}. \tag{1.25}$$

where η is the entropy calculated from the mean thermodynamic quantities in the considered cell, γ is the adiabatic constant, $C_v = \frac{d\epsilon}{dT}|_\rho$ is the specific heat and $f^i = \frac{V_i}{V}$ is the fraction of volume corresponding to the $\mathcal{T}_i$ triangle.

These considerations lead us to define subzone entropy : φ is a subzone entropy if it satisfies the two following conditions.

i) φ is a regular concave function of $\mathbf{f}$.

ii) Whatever the volume fraction f^i so that $f^i \to 0^+$, $\varphi(\mathbf{f}) \to -\infty$.

It is explained in [Després and Labourasse, 2012] how to modify the solver in order to impose the growth of $\overline{\eta}$, while keeping all the properties of the original scheme. Thus, the solver mechanically opposes cell tangling because it would involve $\overline{\eta} \to -\infty$.

Subzone entropy has been essential for us to complete a number of numerical studies. Figure 1.4 illustrates a possible use of subzone entropy in the context of the growth of Richtmyer-Meshkov [Richtmyer, 1960b] instability (we wish to keep the Lagrangian interface as long as possible).

It also remains to study the 3D extension of the method, which, if it does not pose a theoretical problem, certainly requires a great deal of implementation work.

1.8 Non-conforming meshes

in collaboration with A. Claisse, B. Després and F. Ledoux

In the article [Claisse et al., 2012], we extend centered schemes to semi-conforming meshes. The principle, simple but clever, is to redefine the divergence operator (Section 1.3) by injecting the geometrical constraint for the nonconformity vertices in the formula.

If for instance the vertex of coordinates $\mathbf{x}_s$ is constrained to remain in the middle of the vertices of coordinates $\mathbf{x}_k$ and $\mathbf{x}_l$, the variation of the volume V of a cell containing this vertex with respect to the position of the point is written

$$dV(\mathbf{x}_s) = \mathbf{C}_s \cdot d\mathbf{x}_s = \mathbf{C}_s \cdot \left(\frac{d\mathbf{x}_k}{2} + \frac{d\mathbf{x}_l}{2} \right).$$

The formula for the velocity can be deduced from this

$$V'(t) = \sum_{r \ free} \mathbf{C}_r \cdot \mathbf{u}_r + \mathbf{C}_s \cdot \left(\frac{\mathbf{u}_k}{2} + \frac{\mathbf{u}_l}{2} \right),$$

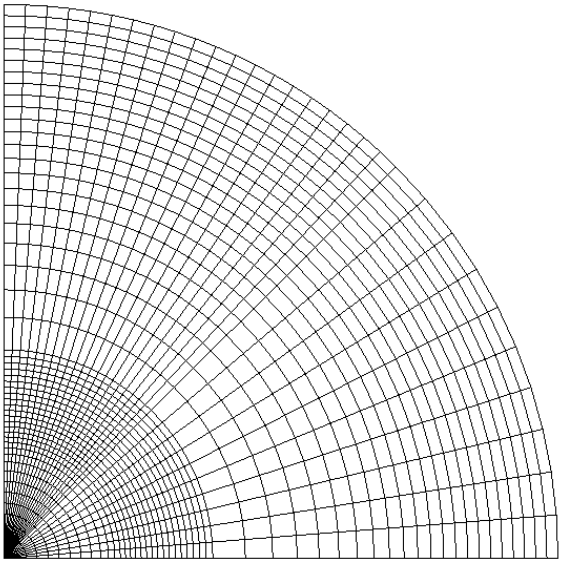

Figure 1.5: Illustration of the use of curved meshes for a cylindrical sod shock tube.

considering that s is the only point of nonconformity in this cell, and where $r\ free$ accounts for the free nodes used in the definition of the volume. As before, a general formula for divergence and gradient is deduced from this:

$$\int_j \nabla \cdot \mathbf{f} \approx \sum_{r\ free} \mathbf{C}_{jr} \cdot \mathbf{f}_r + \mathbf{C}_{js} \cdot \left(\frac{\mathbf{f}_k}{2} + \frac{\mathbf{f}_l}{2} \right),$$

and

$$\int_j \nabla f \approx \sum_{r\ free} \mathbf{C}_{jr} f_r + \mathbf{C}_{js} \left(\frac{f_k}{2} + \frac{f_l}{2} \right).$$

Once these operators are defined, the construction of the scheme is identical to that described in Section 1.3.

This construction method can be generalized to any form of linear dependence of the position of the s point, and is therefore not restricted to nonconformity located on the edge considered (and even less in its middle). For that, it is enough to define $P_1(\mathbf{x}, \mathbf{y}) \in \mathbb{R}^{d \times d}$ and $P_2(\mathbf{x}, \mathbf{y}) \in \mathbb{R}^{d \times d}$ linearly, such that $P_1 + P_2 = Id$. We then get for the divergence (for example):

$$\int_j \nabla \cdot \mathbf{f} \approx \sum_{r\ free} \mathbf{C}_{jr} \cdot \mathbf{f}_r + \mathbf{C}_{js} \cdot (P_1 \mathbf{f}_k + P_2 \mathbf{f}_l).$$

In the article [Claisse et al., 2012], it is further explained how to use this methodology to extend the Glace and Eucclhyd schemes to cells of any shape (no longer only defined as polygons with straight edges, but also with curved edges).

1.9 Angular momentum

in collaboration with B. Després

We report here a work published in 2015 [Després and Labourasse, 2015], whose objective was to estimate the contribution for our applications of a variant of centered schemes preserving the angular momentum at the discrete level.

Indeed the angular momentum

$$\mathbf{w} = \mathbf{u} \wedge \mathbf{x} \tag{1.26}$$

is solution of a conservation law

$$\partial_t(\rho \mathbf{w}) + \nabla \cdot (\rho \mathbf{u} \otimes \mathbf{u} \wedge \mathbf{x}) + \mathbf{rot}(p\mathbf{x}) = 0. \tag{1.27}$$

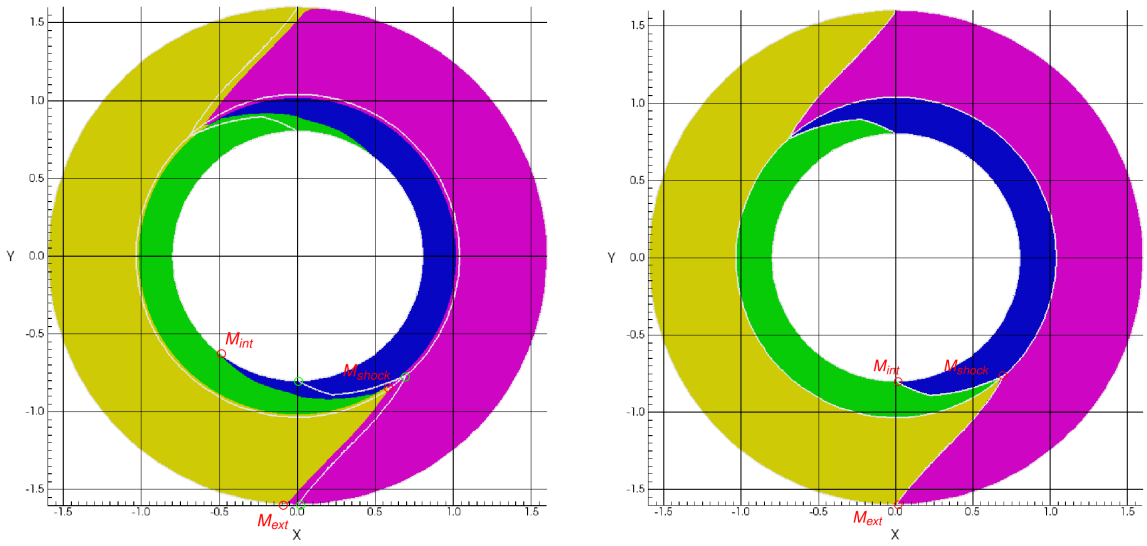

Figure 1.6: Rotating cylindrical shock tube. The colours reflect the deformation of the materials. The white line corresponds to the converged position of the interfaces at the time considered. **On the left** : the non-conservative angular moment scheme does not allow to capture this position. **Right** : the conservative angular momentum scheme allows it.

At the continuous level, this conservation law is redundant with the conservation of the momentum

$$\partial_t(\rho \mathbf{u}) + \nabla \cdot (\rho \mathbf{u} \otimes \mathbf{u}) + \nabla p = 0. \tag{1.28}$$

However, the semi-discrete angular momentum balance is written as follows

$$m_j \frac{d}{dt}\mathbf{w}_j = -\sum_r \mathbf{F}_{jr} \wedge \mathbf{x}_j + m_j \frac{d}{dt}\mathbf{x}_j \wedge \mathbf{u}_j, \tag{1.29}$$

where $\mathbf{x}_j = \frac{1}{V_j}\int_j \mathbf{x}$ is the mass center of the cell. If we sum (1.29) over all cells, one gets

$$\sum_j m_j \frac{d}{dt}\mathbf{w}_j = -\sum_j \sum_r \mathbf{F}_{jr} \wedge \mathbf{x}_j + \sum_j m_j \frac{d}{dt}\mathbf{x}_j \wedge \mathbf{u}_j. \tag{1.30}$$

Since neither term on the right-hand side is generically null, centered schemes are not natively conservative in angular momentum.

To solve this problem, we have added angular momentum $\mathbf{w}_j$ as a discrete unknown to our system. This new variable verifies the semi-discrete conservation law. Indeed

$$\sum_j m_j \frac{d}{dt}\mathbf{w}_j = -\sum_j \sum_r \mathbf{F}_{jr} \wedge \mathbf{x}_r, \tag{1.31}$$

$$= \sum_r \mathbf{x}_r \wedge \sum_j \mathbf{F}_{jr}, \tag{1.32}$$

$$= \mathbf{0}, \tag{1.33}$$

Because the Riemann solver enforces $\sum_j \mathbf{F}_{jr} = \mathbf{0}$. This way, we have a conservation law for the angular momentum $\mathbf{w}$, but with no connection to the velocity field $\mathbf{u}$.

To overcome this difficulty, we propose to add a degree of freedom to the algorithm, by enriching the velocity field

$$\mathbf{v}_j(\mathbf{x}) = \mathbf{a}_j + \mathbf{b}_j \wedge \mathbf{x}. \tag{1.34}$$

where $\mathbf{a}_j$ and $\mathbf{b}_j$ are constant by cell fields. As a result, the enhanced velocity field is composed of all rigid body movements. Obviously, if $\mathbf{b}_j = \mathbf{0}$, $\forall j$, that is to say that only the translations are

taken into account, we recover the classical approximation constant by cell of the Glace or Eucclhyd scheme of order 1.

The corresponding average velocity is defined as

$$\begin{aligned}\mathbf{u}_j &:= \frac{1}{V_j}\int_j \mathbf{a}_j + \mathbf{b}_j \wedge \mathbf{x},\\ &= \mathbf{a}_j + \mathbf{b}_j \wedge \mathbf{x}_j.\end{aligned} \tag{1.35}$$

We also deduce that $\mathbf{w}_j$

$$\begin{aligned}\mathbf{w}_j &:= \frac{1}{V_j}\int_j (\mathbf{a}_j + \mathbf{b}_j \wedge \mathbf{x}) \wedge \mathbf{x},\\ &= (\mathbf{a}_j + \mathbf{b}_j \wedge \mathbf{x}_j) \wedge \mathbf{x}_j + \frac{1}{V_j}\int_j (\mathbf{b}_j \wedge (\mathbf{x} - \mathbf{x}_j)) \wedge (\mathbf{x} - \mathbf{x}_j).\end{aligned} \tag{1.36}$$

In the following, we call $0 < \mathcal{H}_j = \mathcal{H}_j^t \in \mathbb{R}^{d\times d}$ the non-negative definite symmetric matrix

$$\forall \mathbf{b} \in \mathbb{R}^d, \quad (\mathcal{H}_j \mathbf{b}, \mathbf{b}) := \frac{1}{V_j}\int_j |\mathbf{b} \wedge (\mathbf{x} - \mathbf{x}_j)|^2. \tag{1.37}$$

By construction $|\mathcal{H}_j| = O(h^2)$ where h is the characteristic length of the mesh. Thus, the second term in the right-hand side of the equation (1.36) is a second-order correction of the angular momentum.

With these notations (1.36) rewrites

$$\mathbf{w}_j = \mathbf{u}_j \wedge \mathbf{x}_j - \mathcal{H}_j \mathbf{b}_j. \tag{1.38}$$

The formula (1.34) can be used to define the mean total energy

$$\begin{aligned}E_j &:= e_j + \frac{1}{V_j}\int_j \frac{|\mathbf{v}_j(\mathbf{x})|^2}{2},\\ &= e_j + |\mathbf{u}_j|^2/2 + \mathcal{H}_j \mathbf{b}_j \cdot \mathbf{b}_j/2.\end{aligned} \tag{1.39}$$

One more time $\mathcal{H}_j \mathbf{b}_j \cdot \mathbf{b}_j$ is a second-order correction of the total energy E_j.

As $\mathcal{H}_j$ is non-singular, physical variables $\mathbf{u}_j$, $\mathbf{w}_j$ can be inferred bijectively from the couple $\mathbf{a}_j$, $\mathbf{b}_j$

$$\begin{cases}\mathbf{b}_j &= \mathcal{H}_j^{-1}(\mathbf{u}_j \wedge \mathbf{x}_j - \mathbf{w}_j),\\ \mathbf{a}_j &= \mathbf{u}_j - \mathbf{b}_j \wedge \mathbf{x}_j.\end{cases} \tag{1.40}$$

Thus a natural extension of the scheme (1.13) is

$$\begin{cases} m_j \dfrac{d}{dt}\tau_j &= \displaystyle\sum_r \mathbf{C}_{jr} \cdot \mathbf{u}_r,\\ m_j \dfrac{d}{dt}\mathbf{u}_j &= -\displaystyle\sum_r \mathbf{F}_{jr},\\ m_j \dfrac{d}{dt}\mathbf{w}_j &= -\displaystyle\sum_r \mathbf{F}_{jr} \wedge \mathbf{x}_r.\\ m_j \dfrac{d}{dt}E_j &= -\displaystyle\sum_r \mathbf{F}_{jr} \cdot \mathbf{u}_r.\end{cases} \tag{1.41}$$

This system is closed by the equations (1.40) for the reconstructed field, the equation (1.39) to recalculate the internal energy, and by the equations of state for the pressure. It remains to calculate the new fluxes as in the equation (1.14), taking into account the enriched field.

In conclusion, this study shows that a significant gain in accuracy can be obtained by preserving angular momentum. However, this is at the cost of a loss of the semi-discrete entropy condition, and does not change the order of the scheme.

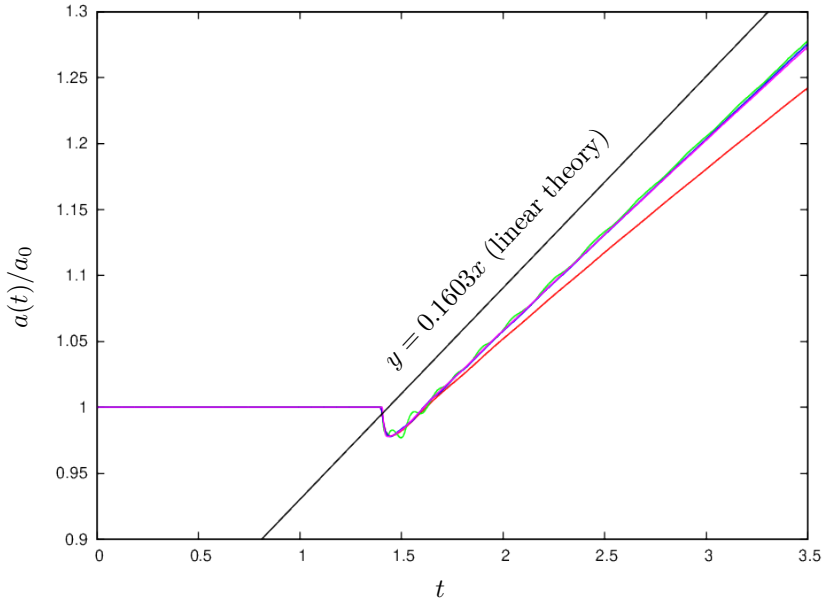

Figure 1.7: Growth rate of linear-phase Richtmyer-Meshkov instability for a Mach number of $\approx 3 \times 10^{-2}$. The red curve is the result of the standard scheme. The blue and green curves correspond to the results obtained with the entropy stable modified scheme (blue) or non-entropy stable modified scheme (green). The purple curve corresponds to the result of the standard scheme on a mesh twice as fine, and the black line to the linear theory [Clarisse et al., 2004]. On notes the marked improvement in accuracy with the correction.

1.10 Low-Mach correction

The low-Mach regime corresponds to the quasi-incompressible limit of the compressible Euler equations. In this regime, it is shown that most of the schemes dedicated to the capture of shocked solutions suffer from a redhibitory numerical dissipation (see for example [Dellacherie, 2010]). To study this regime, it is convenient to put the system of Euler equations in dimensionless form using the scaling:

$$\overline{\mathbf{x}} = \frac{\mathbf{x}}{L},\ \overline{t} = \frac{t}{t_R},\ \overline{\rho} = \frac{\rho}{\rho_R},\ \overline{p} = \frac{p}{p_R},\ \overline{\mathbf{u}} = \frac{\mathbf{u}}{u_R},\ \overline{E} = \frac{E}{e_R}, \overline{c} = \frac{c}{c_R}$$

where the parameters $L, t_R, \rho_R, p_R, u_R = L/t_R, E_R = p_R/\rho_R$ and $c_R = \sqrt{p_R/\rho_R}$ are respectively the length, time, density, pressure, velocity, energy and sound speed characteristic of the flow. The characteristic Mach number is deduced from this $M = u_R/c_R$.

The system of Euler's equations in Lagrangian formulation then becomes:

$$\begin{aligned}
\overline{\rho} D_{\overline{t}} \overline{\tau} - \nabla \cdot \overline{\mathbf{u}} &= 0, \\
\overline{\rho} D_{\overline{t}} \overline{\mathbf{u}} + \frac{1}{M^2} \nabla \overline{p} &= \mathbf{0}, \\
\overline{\rho} D_{\overline{t}} \overline{E} + \nabla \cdot (\overline{p} \overline{\mathbf{u}}) &= 0,
\end{aligned}$$

with $\overline{E} = \overline{e} + M^2 \overline{\mathbf{u}}^2/2$.

Within the framework of the centered schemes described in this report, it can be shown that under conditions of low compressibility, the schemes Eucclhyd [Maire et al., 2007b], Glace [Després and Mazeran, 2005] and CCH [Burton et al., 2013b] are consistent in the weak sense with the following

dimensionless system:

$$
\begin{aligned}
d_{\overline{t}} \int_j 1 &= \int_j \nabla \cdot \overline{\mathbf{u}} + O(\overline{h}), \\
d_{\overline{t}} \int_j \overline{\rho \mathbf{u}} &= -\int_j \frac{1}{M^2} \nabla \overline{p} + O(\frac{\overline{h}}{M}), \\
d_{\overline{t}} \int_j \overline{\rho e} &= -\int_j \nabla \cdot (\overline{p \mathbf{u}}) + O(\overline{h}).
\end{aligned}
\tag{1.42}
$$

There is an error of the order of $O(\frac{\overline{h}}{M})$ on the momentum balance, which tends towards infinity as the flow approaches the incompressible limit.

To correct this problem, a modification of the scheme [Labourasse, 2019] has been proposed. The new semi-discrete in space scheme is written

$$
\begin{aligned}
\frac{d}{dt} \int_j 1 &= \sum_r \mathbf{C}_{jr} \cdot \mathbf{u}_r, \\
\frac{d}{dt} \int_j \rho \mathbf{u} &= -\sum_r \sum_f \mathbf{G}_{jr}, \\
\frac{d}{dt} \int_j \rho E &= -\sum_r \sum_f \mathbf{G}_{jr} \cdot \mathbf{u}_r,
\end{aligned}
\tag{1.43}
$$

with $\mathbf{G}_{jr} = \lambda_r \mathbf{F}_{jr} + (1 - \lambda_r)\mathbf{H}_{jr}$, $\lambda_r \in [0\ 1] \subset \mathbb{R}$, and $\mathbf{H}_{jr} = \mathbf{C}_{jr} p_r$. The term p_r is a consistent estimate of the vertex pressure which does not depend on M. It is then shown that if the coefficient λ_r is proportional to the local Mach number, the previous precision problem is solved. We also show that λ_r can be chosen so as to preserve the semi-discrete growth of entropy. The effect of this correction on the growth rate of an Richtmyer-Meshkov instability is illustrated on the figure 1.7.

Mr Churchill, to what do you attribute your success in life?
***Conservation of energy**. Never stand up when you can sit down. And never sit down when you can lie down.*

Winston Churchill

2

Numerical methods for radiative diffusion

2.1 Introduction

This chapter describes the work carried out to solve phase II of the main introduction, i.e. radiation diffusion with frozen hydrodynamics. It is recalled that by using a elementary change of variable, the problem (20) has been brought back in the form of a non-linear parabolic equation (23)

$$\frac{\partial}{\partial t}X = \alpha(X)\nabla\cdot\beta(X)\nabla X.$$

where $X = T^{\xi}$, with ξ a well-chosen real, so that the function $\beta(X) > 0$ has little dependency on X, and $\alpha(X) > 0$. This change of variable is valid provided that $T > 0$, which is also the condition recalled in introduction, for the system to admit physically admissible solutions. Time discretization is necessarily implicit or semi-implicit to avoid a parabolic CFL condition. It can be performed by an implicit Euler (order 1) or Crank-Nicolson (order 2) scheme. In any case, we end up with a problem to be solved at each iteration of the form

$$X^{n+1} = \lambda(X^{n+1},\Delta t)\nabla\cdot\beta(X^{n+1})\nabla X^{n+1} + h(X^n,\Delta t),$$

where $h(X,\Delta t) > 0, \forall X > 0, \Delta t > 0$ and $\lambda(X^\nu,\Delta t) > 0$ is a linear function of $\alpha(X^{n+1})$ and of the time step Δt. This problem is not directly solvable, and a Newton or fixed-point procedure is used to cope with the non-linearity. In each ν iteration of this procedure, we solve an equation of the form

$$X^{\nu+1} = \lambda(X^\nu,\Delta t)\nabla\cdot\beta(X^\nu)\nabla X^{\nu+1} + h(X^n,\Delta t).$$

In order to be able to inverse the change of variable, and return to the physical variable T, it is necessary and sufficient that $X^{\nu+1} > 0$. This means that

$$\lambda(X^\nu,\Delta t)\nabla\cdot\beta(X^\nu)\nabla X^{\nu+1} + h(X^n,\Delta t) > 0.$$

A sufficient condition for this is that the equation

$$\lambda(X^\nu,\Delta t)\nabla\cdot\beta(X^\nu)\nabla X^{\nu+1} + h(X^n,\Delta t) = 0,$$

combined with boundary conditions, has a unique positive solution. In order to lighten the notations, we therefore consider the following model. Solve

$$\begin{cases} -\nabla\cdot(\kappa\nabla u) = f, & \text{in } \Omega, \\ \gamma\,(\kappa\nabla u)\cdot n + \delta u = g & \text{on } \partial\Omega, \end{cases} \tag{2.1}$$

where Ω is an open set of $\mathbb{R}^2$, n is the outgoing normal to Ω. The data verify $f \in L^2(\Omega)$, $g \in H^{1/2}(\partial\Omega)$, and $\kappa \in L^\infty(\Omega)$ satisfies the ellipticity condition

$$\forall x \in \Omega, \quad \kappa(x) \geq \kappa_0 > 0.$$

The functions γ and δ are smooth and so that

$$\forall x \in \partial\Omega, \quad \delta(x) \geq 0, \quad \text{and} \quad \gamma(x) \geq \gamma_0 > 0.$$

Under the above conditions, one can prove (see [Evans, 1978]) that the system (2.1) has a unique solution in $H^1(\Omega)$. This solution fulfills a maximum principle, i.e. if $m \leq f \leq M$ and $m\delta \leq g \leq M\delta$, then $m \leq u \leq M$. For linear problems, this maximum principle is equivalent to the positivity of the solution ($0 \leq f$ and $0 \leq g$, then $0 \leq u$), whereas for non-linear problems, this positivity is only induced. The positivity is thus a weaker property. However, it is sufficient to ensure the constraint $u > 0$ and thus $T > 0$. Our objective is thus to find a discretization of (2.1) that respects at the discrete level the positivity property of the solution.

The perfect scheme has the following properties: it is consistent (ideally of order greater than or equal to 2), stable, conservative, and verifies the maximum principle (or at least the positivity) at the discrete level. It is also linear and produces a symmetric matrix. Finally, it relies on a reduced stencil so that the parallelization is effective, and it couples easily with the scheme described in the previous section, i.e. it operates on the the average value of u (function of T) in each volume of control (cell).

In summary, it has the following characteristics:

1. consistence;
2. order 2;
3. stability;
4. conservation;
5. small stencil (in link with parallelization);
6. positivity;
7. maximum principle;
8. symmetry;
9. linearity;
10. finite volumes.

Unfortunately, there is currently no scheme checking all these properties. The properties on which it is not possible to compromise are 1, 3 and 4. The property 5 is not absolutely blocking, but if the stencil of the scheme depends on the mesh, its parallelization becomes a very complex task that one wishes to avoid. The properties 2, 7, 8 and 9, are desirable but not mandatory.

The previous analysis suggests that at least positivity 6 is an indispensable property in our applications. On the other hand, most of our problems being by nature non-linear, their resolution requires an iterative procedure. We explain later why this characteristic decreases the importance of the property 9. We also explain why we have privileged finite volume schemes 10.

Background To explain the choice of this new scheme, we propose a quick and critical inventory of the methods available in the literature.

Finite elements (see [Ciarlet, 2002b]) are the most popular discretization of the diffusion operator. This possibility has been discarded because of the point 10 in the ideal scheme described above. From the order 2, finite elements require several degrees of freedom per cell, which makes them difficult to couple with hydrodynamics (phase I).

We are therefore interested in finite volume methods (or which can be interpreted as such), to which a significant number of works are dedicated. All the methods presented below thus check the property 10. Without claiming to be exhaustive, here are the main possibilities we have explored (see the journal article [Droniou et al., 2009] for more details):

Kershaw The first scheme envisaged (and at our knowledge, one of the first published) is the work of Kershaw [Kershaw, 1981] (see also [Pert, 1981] for a close scheme). This scheme is based on an isoparametric transformation of the cell into an ideal element. This scheme verifies the properties 3, 4, 5, 8, 9 and 10 of our ideal scheme. Unfortunately, it can only be proven to be consistent on parallelogram meshes. Moreover, it does not respect the maximum principle (or positivity). This is why it has been discarded.

Diamond The so-called "diamond" schemes have been analysed in [Coudière et al., 1999], and are the basis of the scheme that we chose. An auxiliary unknown located at the vertices of the cell is added. The value of this unknown is a function of the values taken by the main unknown. This makes it possible to calculate a second-order flux approximation. The overall order of this method depends on the interpolation formula of the auxiliary unknowns from the main unknowns. If this one is sufficiently precise, we obtain a scheme of order 2. Generically, this method verifies the properties 1, 2, 3, 4, 5, 9 et 10.

DDFV More recently, F. Hermeline proposed the method DDFV[1] [Hermeline, 1998, 2000, 2003, 2007, 2008, 2009]. F. Hermeline adopts the idea of adding localized auxiliary unknowns at the tops of the mesh. However, the values of these unknowns are not deduced from the values of the main unknown, but are solution of a second elliptical problem (2.1) discretized on the dual mesh. Two diffusion problems are thus solved jointly, the auxiliary unknown of one being the main unknown of the other one. This method converges to the second-order, even if the mesh contains non-convex elements. It is therefore a robust and accurate method that verifies the properties 1, 2, 3, 4, 5, 8, 9 and 10. As with finite element methods, the main problem with this method is that the addition of this auxiliary variable makes it difficult to couple it to other physical models. Moreover, it does not verify the maximum principle, nor the positivity (however, a recent extension of the scheme [Camier and Hermeline, 2016] makes it possible to guarantee the positivity).

Mimetic The so-called "mimetic" schemes are described in [Brezzi et al., 2009, 2005, Lipnikov et al., 2006, Kuznetsov et al., 2005] (this work is summarized in the review paper [Lipnikov et al., 2014a]). The design principle of these schemes is to mimic at the discrete level some of the properties of the continuous scheme. In particular, the authors discreetly reproduce the duality between the gradient operator and the divergence operator. This method satisfies the properties 1, 2, 3, 4, 5, 8, 9 and can be reinterpreted as a finite volume method (10). However, it suffers from a lack of robustness (no maximum principle or discrete positivity [Lipnikov et al., 2011]), and the number of degrees of freedom is greater than that of the other methods (fluxes are considered additional unknowns).

Sushi The SUSHI [Eymard et al., 2010] scheme based on the same principles as **Diamond** proposes to add stabilization to improve robustness. However, this stabilization does not preserve the maximum principle (and not the positivity either). In [Droniou et al., 2010] and especially [Droniou et al., 2016, 2018], these last three schemes (DDFV, Mimetic and SUSHI) are grouped in a family called **gradient schemes**. They all verify the properties 1, 3, 4, 5, 8, 9 and 10.

MPFA The multi-point flux approximation (MPFA) [Aavatsmark et al., 2007, Breil and Maire, 2007, Edwards and Rogers, 1998] uses auxiliary unknowns at the edges of the mesh. These unknowns are used to calculate a consistent approximation of the flux, and are eliminated by requiring that the flux is continuous through the edges. This method is available in several variants. Depending on the variants, the following pathologies can be observed: either the local matrix used to eliminate auxiliary unknowns is singular on certain meshes, either the method does not not converge on random meshes. In any case, the principle of maximum is not satisfied (see [Eigestad et al., 2002, Friis and Edwards, 2011, Edwards and Zheng, 2008]), and neither

[1] Discrete Duality Finite Volume.

is positivity. To summarize these schemes check the properties 1 and 2 **or** 3 and 4, 5, 8, 9 and 10.

Le Potier In [Le Potier, 2009], a finite differences scheme is proposed by Le Potier. This scheme, which can be reinterpreted as a finite volume scheme, is of order 1 and verifies the maximum principle. Unfortunately, it requires to enlarge the stencil in a significant and mesh-dependent way. This makes its use in a parallel Lagrangian framework (domain decomposition) very complicated. This scheme verifies the properties 1, 3, 4, 6, 7, 9 and 10.

Lapin In [Siess, 2009], Siess proposes a linear finite volume scheme of order 1 which satisfies the maximum principle. The principle of this scheme is to construct the Voronoï mesh. On this mesh the TPFA scheme (refer for instance to [Droniou et al., 2018] for an analysis of this scheme), is consistent, of order 2 and verify the maximum principle. However, the passage from the initial mesh to the associated Voronoï mesh induces a order 1 error at the end. This scheme verifies the properties 1, 3, 4, 5, 7, 8, 9 and 10, which makes it a credible candidate. The problem is that the stencil induced by this method depends on the mesh (even if local) and the extension to anisotropic diffusion remains to be explored.

DLP In [Droniou and Le Potier, 2011], a non-linear scheme is constructed, which uses auxiliary unknowns to compute consistent fluxes. The positions of these unknowns are not explicitly defined in the paper, but must belong to the perpendicular to the edge passing through the center of the considered cell. Droniou and Le Potier revisit the original idea of Bertolazzi and Manzini [Bertolazzi and Manzini, 2005] which is to construct a consistent flux in each cell sharing an edge. The final flux is obtained by convex combination and leads to a scheme of order 2 which verifies the maximum principle. The coefficients of this convex combination depend on the unknown, which makes the scheme non-linear. A large part of these principles are included in the scheme described in this document. One of the main problems of this scheme is that the method to consistently evaluate the auxiliary unknowns is not local, and therefore difficult to parallelize. The **DLP** method then fulfill properties 1, 2, 3, 4, 6, 7 et 10, and was part of our evaluation (see below).

SY Sheng and Yuan propose in [Sheng and Yuan, 2011], a very similar scheme, but which explicitly defines the position of the auxiliary unknowns in the middle of the edges of the mesh. As in the previous method, the interpolation of the auxiliary unknowns values is not local, and this scheme fulfills the properties 1, 2, 3, 4, 6, 7 and 10, and was part of our evaluation (see below).

SYY The scheme proposed in [Sheng et al., 2009, Wang et al., 2012, Yuan and Sheng, 2008] is based on the same idea. A non-linear and consistent flux is constructed by convex combination of two consistent fluxes. However, this convex combination ensures only the positivity of the scheme and not the maximum principle. On the other hand, we formally obtain a two-point flux as in the TPFA scheme, which allows to decrease the bandwidth of the matrix to be inverted (a similar method is proposed in [Lipnikov et al., 2007]). Following the example of the previous method, the interpolation of the auxiliary unknowns is not local, and this scheme fulfills properties 1, 2, 3, 4, 6, and 10, and was part of our evaluation (see below).

LSV Finally, it should be noted that positive schemes have been developed, also based on a convex combination of consistent flows, but which do not require auxiliary unknowns [Lipnikov et al., 2012, 2010, Nikitin and Vassilevski, 2010, Lipnikov et al., 2009b, Danilov and Vassilevski, 2009]. However, for deformed meshes, the stencil must be extended, which makes the parallelization a delicate task. These schemes fulfill the properties 1, 2, 3, 4, 6, and 10.

A study was conducted to try to reconcile robustness and precision for the diffusion operator. It led to the Master 2 internship of Samuel De Santis [De Santis, 2011], who evaluated the previously mentioned schemes. These schemes [Bertolazzi and Manzini, 2007b, Droniou and Le Potier, 2011, Sheng et al., 2009, Sheng and Yuan, 2011] are **consistent** and at least **positif** ([Bertolazzi and Manzini, 2007b, Droniou and Le Potier, 2011, Sheng and Yuan, 2011] also respect the maximum principle). In return for these very good properties, they induce an additional non-linearity to the problem (in particular they require to solve a non-linear problem, even for a linear diffusion equation), and do not lead to a symmetric matrix (which prohibits the use of some efficient iterative solvers

such as the conjugate gradient). During the internship, we compared the schemes proposed in the literature and decided to take inspiration from the scheme described in [Sheng et al., 2009]. In our tests, this scheme is the most accurate and the one for which the non-linear problem converges the fastest. On the other hand, it's only **positive** (it does not respect the maximum principle). We've considered the **positivity** to be sufficient to ensure the robustness of the calculations. Another advantage of this choice, is that even if the flux obtained by this scheme is indeed **multi-point**, the partial explicitation of this flux formally induces a **two points flux** in the matrix of the problem. That leads to sparser matrices, and so *a priori* more easy to invert. We have also developed a new method of interpolation of auxiliary unknowns, making it possible to preserve the locality of the scheme (reduced stencil). The scheme described hereafter and in [Blanc and Labourasse, 2016] fulfills so properties 1, 2, 3, 4, 5, 6 and 10.

2.2 Positive scheme for radiative diffusion

in collaboration with X. Blanc

The main lines of construction of the scheme are described in this section. It is largely inspired by [Yuan and Sheng, 2008]. The differences concern the boundary conditions (not described in this document) and the evaluation of auxiliary unknowns. Demonstrations of the properties of the scheme are not detailed, and the interested reader may refer to [Blanc and Labourasse, 2016].

In the following we note

- $\mathcal{K}$ the set of the cells of the mesh;
- $\mathcal{E}$ the set of the edges of the mesh;
- $\mathcal{N}$ the set of the vertices of the mesh;

For all $K \in \mathcal{K}$, we denote K the center of this cell. For all $L \in \mathcal{K}$ sharing an edge with K, we denote $e = K|L \in \mathcal{E}$ the common edge.

For an edge e of a cell K, we denote $\mathbf{n}_{K,e}$ the outgoing normal with respect to K to the edge e. Finally, we define the characteristic length scale of the mesh

$$\Delta x = \max\{|e|, \quad e \in \mathcal{E}\}. \tag{2.2}$$

2.2.1 Discrete fluxes

To write a finite volume scheme for (2.1), we integrate the equations on a cell K:

$$-\int_K \nabla \cdot (\kappa \nabla u) dx = \int_K f dx,$$

and use the Green formula:

$$-\int_{\partial K} \kappa \nabla u \cdot \mathbf{n}_{K,e} d\Gamma = \int_K f dx.$$

Using the assumption that the cells are polygons, we can write the previous equation equivalently

$$\sum_{e \in \partial K} \left(-\int_e \kappa \nabla u \cdot \mathbf{n}_{K,e} d\Gamma \right) = \int_K f dx. \tag{2.3}$$

In the following, we denote

$$\mathcal{F}_{K,e} = -\int_e \kappa(x) \nabla u(x,t) \cdot \mathbf{n}_{K,e} d\Gamma,$$

the outgoing flux of K through the edge e. The objective is to construct an approximation of $\mathcal{F}_{K,e}$ for each edge e, as a function of the unknowns (volume means per cell).

To do this, we introduce auxiliary unknowns at the vertices of the mesh. We then define the points M_1 and M_2, as the vertices of K such as the basis $(\mathbf{KM_1}, \mathbf{KM_2})$ is direct, and such that the decomposition of $\mathbf{n}_{K,e}$ in this basis gives positive coordinates. Figure 2.1 illustrates this choice. The

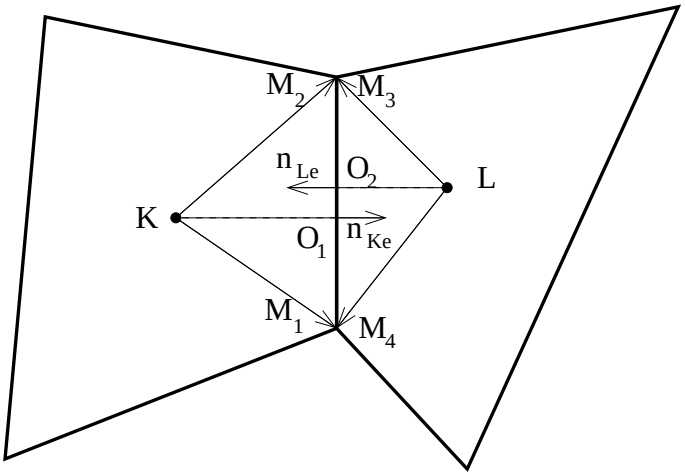

Figure 2.1: The cells K and L, their centers, and the points M_i for $1 \leq i \leq 4$.

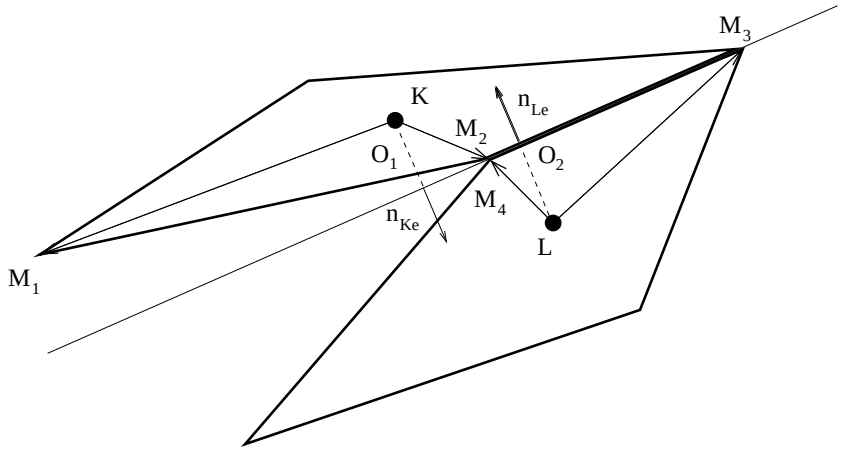

Figure 2.2: The cells K, L and the points M_i for $1 \leq i \leq 4$ in the case where these points do not correspond to the vertices of the edge $e = K|L$.

points M_3 and M_4 are defined in the same way, with the constraint that the basis $(\mathbf{LM_3}, \mathbf{LM_4})$ is direct, and that the decomposition of the vector $\mathbf{n}_{L,e}$ in this basis, gives positive coordinates. We define O_1 (respectively O_2), the intersection between the half-line from K (respectively L) in the direction $\mathbf{n}_{K,e}$ (respectively $\mathbf{n}_{L,e}$) and the border of K (respectively from L). We also define the angles

$$\theta_{K_1} = (\mathbf{KM_1}, \mathbf{KO_1}), \quad \theta_{K_2} = (\mathbf{KO_1}, \mathbf{KM_2}), \quad \theta_{L_1} = (\mathbf{LM_3}, \mathbf{LO_2}), \quad \theta_{L_2} = (\mathbf{LO_2}, \mathbf{LM_4}),$$

$$\theta_K = \theta_{K_1} + \theta_{K_2}, \quad \theta_L = \theta_{L_1} + \theta_{L_2}.$$

Note that the M_i points are not necessarily the vertices of the edge e (see Figure 2.2). We can then write the vector $\mathbf{n}_{K,e}$ as a linear combination of $\mathbf{KM_1}$ and $\mathbf{KM_2}$. It allows us to determine $\alpha \in \mathbb{R}$ and $\beta \in \mathbb{R}$ so that

$$\mathbf{n}_{K_e} = \alpha \frac{\mathbf{KM_1}}{\|\mathbf{KM_1}\|} + \beta \frac{\mathbf{KM_2}}{\|\mathbf{KM_2}\|}. \tag{2.4}$$

We calculate the wedge product of (2.4) with $\mathbf{KM_1}$, which induces

$$\left.\begin{array}{ll} \|\mathbf{n}_{K_e} \wedge \mathbf{KM_1}\| & = \|\mathbf{KM_1}\| \, |\sin\theta_{K_1}| \\ \|\mathbf{n}_{K_e} \wedge \mathbf{KM_1}\| & = |\beta| \, \|\mathbf{KM_1}\| \, |\sin\theta_K| \end{array}\right\} \Longrightarrow |\beta| = \left|\frac{\sin\theta_{K_1}}{\sin\theta_K}\right|.$$

As $\theta_K \in (0,\pi]$ and $\theta_{K_1} \in (0,\pi]$, we have $0 < \sin\theta_K \leq 1$ and $0 < \sin\theta_{K_1} \leq 1$ and then

$$0 < \beta \left(= \frac{\sin\theta_{K_1}}{\sin\theta_K} \right) \leq 1.$$

Likewise, $\alpha = \dfrac{\sin\theta_{K_2}}{\sin\theta_K}$. Then, we have

$$\mathbf{n}_{K_e} = \frac{\sin\theta_{K_2}}{\sin\theta_K} \frac{\mathbf{KM_1}}{\|\mathbf{KM_1}\|} + \frac{\sin\theta_{K_1}}{\sin\theta_K} \frac{\mathbf{KM_2}}{\|\mathbf{KM_2}\|}. \tag{2.5}$$

A similar argument gives us

$$\mathbf{n}_{L_e} = \frac{\sin\theta_{L_2}}{\sin\theta_L} \frac{\mathbf{LM_3}}{\|\mathbf{LM_3}\|} + \frac{\sin\theta_{L_1}}{\sin\theta_L} \frac{\mathbf{LM_4}}{\|\mathbf{LM_4}\|}. \tag{2.6}$$

We infer that

$$\mathcal{F}_{K,e} = -\int_e \left(\frac{\sin\theta_{K_2}}{\sin\theta_K} \frac{\nabla u \cdot \mathbf{KM_1}}{\|\mathbf{KM_1}\|} + \frac{\sin\theta_{K_1}}{\sin\theta_K} \frac{\nabla u \cdot \mathbf{KM_2}}{\|\mathbf{KM_2}\|} \right) \kappa(x) d\Gamma,$$
$$\mathcal{F}_{L,e} = -\int_e \left(\frac{\sin\theta_{L_2}}{\sin\theta_L} \frac{\nabla u \cdot \mathbf{LM_3}}{\|\mathbf{LM_3}\|} + \frac{\sin\theta_{L_1}}{\sin\theta_L} \frac{\nabla u \cdot \mathbf{LM_4}}{\|\mathbf{LM_4}\|} \right) \kappa(x) d\Gamma.$$

A Taylor expansion of u tells us that

$$\nabla u \cdot \frac{\mathbf{KM_i}}{\|\mathbf{KM_i}\|} = \frac{u(M_i) - u(K)}{\|\mathbf{KM_i}\|} + O(\Delta x).$$

And then,

$$\mathcal{F}_{K,e} = -|e| \left(\frac{\sin\theta_{K_2}}{\sin\theta_K} \frac{u_{M_1} - u_K}{\|\mathbf{KM_1}\|} + \frac{\sin\theta_{K_1}}{\sin\theta_K} \frac{u_{M_2} - u_K}{\|\mathbf{KM_2}\|} \right) \kappa_e + O(\Delta x^2),$$
$$\mathcal{F}_{L,e} = -|e| \left(\frac{\sin\theta_{L_2}}{\sin\theta_L} \frac{u_{M_3} - u_L}{\|\mathbf{LM_3}\|} + \frac{\sin\theta_{L_1}}{\sin\theta_L} \frac{u_{M_4} - u_L}{\|\mathbf{LM_4}\|} \right) \kappa_e + O(\Delta x^2),$$

where κ_e is a value of $\kappa(x)$ at the middle of edge e. We define

$$F_1 = -|e|\kappa_e \left(\frac{\sin\theta_{K_2}}{\sin\theta_K} \frac{u_{M_1} - u_K}{\|\mathbf{KM_1}\|} + \frac{\sin\theta_{K_1}}{\sin\theta_K} \frac{u_{M_2} - u_K}{\|\mathbf{KM_2}\|} \right), \tag{2.7}$$

$$F_2 = -|e|\kappa_e \left(\frac{\sin\theta_{L_2}}{\sin\theta_L} \frac{u_{M_3} - u_L}{\|\mathbf{LM_3}\|} + \frac{\sin\theta_{L_1}}{\sin\theta_L} \frac{u_{M_4} - u_L}{\|\mathbf{LM_4}\|} \right). \tag{2.8}$$

the second-order accurate approximation of the fluxes $\mathcal{F}_{K,e}$ and $\mathcal{F}_{L,e}$. The way u_{M_i} is calculated is discussed in Section 2.2.2. Determining the value of κ on the edge e is a problem in itself, which is not addressed in this document.

The main idea of these scheme designs has been formulated to our knowledge by Bertolazzi and Manzini [Bertolazzi and Manzini, 2005]. They notice that the formulas (2.7) and (2.8) correspond to two consistent approximations of the same flux $\mathcal{F}_{K,e}$ through the edge e (up to the sign). Consequently, any convex combination of these two approximations results also in a consistent formula for $\mathcal{F}_{K,e}$. We're going to use this degree of freedom to force the positivity of the scheme. To do this, we write

$$F_{K,e} = \mu_1(u)F_1 - \mu_2(u)F_2, \tag{2.9}$$
$$F_{L,e} = \mu_2(u)F_2 - \mu_1(u)F_1, \tag{2.10}$$

where $\mu_1 \in \mathbb{R}$ and $\mu_2 \in \mathbb{R}$. For these new approximations to be consistent, it is necessary to require that $\mu_1 \geq 0$, $\mu_2 \geq 0$, and $\mu_1 + \mu_2 = 1$. To determine μ_1 and μ_2, we need another equation. In the literature, many choices are proposed (see [Droniou and Le Potier, 2011] and [Sheng et al., 2009]) which impacts the properties of the scheme. For the scheme presented here, we have chosen [Sheng

et al., 2009], which results in a two-point flow formulation. Other choices lead to multi-point flows which induce a scheme respecting the maximum principle.

By injecting (2.7) and (2.8) in (2.9) and (2.10), we obtain:

$$\begin{aligned} F_{K,e} &= \mu_1 F_1 - \mu_2 F_2 \\ &= -\mu_1 |e| \kappa_e \left(\frac{\sin\theta_{K_2}}{\sin\theta_K} \frac{u_{M_1} - u_K}{\|\mathbf{KM_1}\|} + \frac{\sin\theta_{K_1}}{\sin\theta_K} \frac{u_{M_2} - u_K}{\|\mathbf{KM_2}\|} \right) \\ &\quad +\mu_2 |e| \kappa_e \left(\frac{\sin\theta_{L_2}}{\sin\theta_L} \frac{u_{M_3} - u_L}{\|\mathbf{LM_3}\|} + \frac{\sin\theta_{L_1}}{\sin\theta_L} \frac{u_{M_4} - u_L}{\|\mathbf{LM_4}\|} \right). \end{aligned}$$

And then,

$$\begin{aligned} F_{K,e} &= \mu_1 |e| \kappa_e \left(\frac{\sin\theta_{K_1}}{\sin\theta_K} \frac{1}{\|\mathbf{KM_2}\|} + \frac{\sin\theta_{K_2}}{\sin\theta_K} \frac{1}{\|\mathbf{KM_1}\|} \right) u_K \\ &\quad -\mu_2 |e| \kappa_e \left(\frac{\sin\theta_{L_1}}{\sin\theta_L} \frac{1}{\|\mathbf{LM_4}\|} + \frac{\sin\theta_{L_2}}{\sin\theta_L} \frac{1}{\|\mathbf{LM_3}\|} \right) u_L \\ &\quad -\mu_1 \underbrace{|e| \kappa_e \left(\frac{\sin\theta_{K_1}}{\sin\theta_K} \frac{u_{M_2}}{\|\mathbf{KM_2}\|} + \frac{\sin\theta_{K_2}}{\sin\theta_K} \frac{u_{M_1}}{\|\mathbf{KM_1}\|} \right)}_{=a_1} \\ &\quad +\mu_2 \underbrace{|e| \kappa_e \left(\frac{\sin\theta_{L_1}}{\sin\theta_L} \frac{u_{M_4}}{\|\mathbf{LM_4}\|} + \frac{\sin\theta_{L_2}}{\sin\theta_L} \frac{u_{M_3}}{\|\mathbf{LM_3}\|} \right)}_{=a_2}. \end{aligned} \tag{2.11}$$

To obtain two-point fluxes, it is necessary to eliminate any reference to the auxiliary variables u_{M_i}. This requires that μ_1 and μ_2 are solutions of the following system:

$$\left\{ \begin{array}{lcl} \mu_1 + \mu_2 & = & 1, \\ a_1\mu_1 - a_2\mu_2 & = & 0. \end{array} \right.$$

As soon as $a_1 + a_2 \neq 0$, this system admits a unique solution, which writes

$$\mu_1 = \frac{a_2}{a_1 + a_2}, \quad \mu_2 = \frac{a_1}{a_1 + a_2}.$$

Thanks to the choice of M_1, M_2, M_3, M_4, (see figures 2.1 and 2.2), $a_1 \geq 0$ and $a_2 \geq 0$ (as soon as $u_{M_i} \geq 0$, see Section 2.2.2). It follows that the constraints $\mu_1 \geq 0$ and $\mu_2 \geq 0$ are automatically satisfied. When $a_1 + a_2 = 0$, [Sheng et al., 2009, Yuan and Sheng, 2008] propose to choice arbitrarily $\mu_1 = \mu_2 = \frac{1}{2}$. However, this may induce a discontinuity in the flux with respect to u. This pathology invalidates some proofs, and that is why we have chosen to compute a_1 and a_2, in a slightly different way, without losing any of the properties of the scheme

$$\tilde{a}_1 = a_1 + \Delta x^2, \quad \tilde{a}_2 = a_2 + \Delta x^2,$$

where Δx is defined for instance by (2.2)[2]. It provides new expressions for μ_1 and μ_2

$$\tilde{\mu}_1 = \frac{a_2 + \Delta x^2}{a_1 + a_2 + 2\Delta x^2}, \quad \tilde{\mu}_2 = \frac{a_1 + \Delta x^2}{a_1 + a_2 + 2\Delta x^2}.$$

We deduce from this the expression of the approximate fluxes

$$\begin{aligned} F_{K,e} = -F_{L,e} = \tilde{\mu}_1 |e| \kappa_e \left(\frac{\sin\theta_{K_1}}{\sin\theta_K} \frac{1}{\|\mathbf{KM_2}\|} + \frac{\sin\theta_{K_2}}{\sin\theta_K} \frac{1}{\|\mathbf{KM_1}\|} \right) u_K \\ - \tilde{\mu}_2 |e| \kappa_e \left(\frac{\sin\theta_{L_1}}{\sin\theta_L} \frac{1}{\|\mathbf{LM_4}\|} + \frac{\sin\theta_{L_2}}{\sin\theta_L} \frac{1}{\|\mathbf{LM_3}\|} \right) u_L. \end{aligned} \tag{2.12}$$

Since we imposed $F_{L,e} = -F_{K,e}$, the scheme is conservative. Moreover the fluxes writes

$$F_{K,e} = -F_{L,e} = A_{K,e} u_K - A_{L,e} u_L,$$

with $A_{K,e} \geq 0$ and $A_{L,e} \geq 0$. It implies that the matrix associated with the scheme is the transpose of a **M-matrix**. Consequently, the scheme is well defined (stability) and positive.

[2] In practice, a local evaluation of the cell diameter is used.

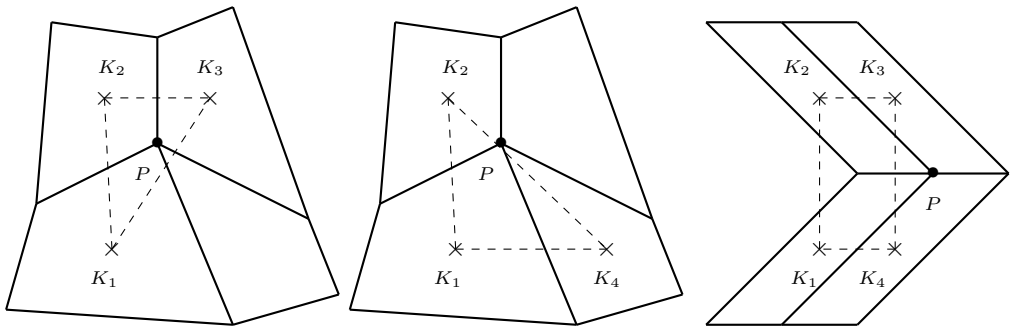

Figure 2.3: Illustration of the problems induced by the interpolation method proposed in [Yuan and Sheng, 2008]. For the two figures on the left, several local possibilities are suitable. For the figure on the right, there is no local possibility to obtain a triangle containing P.

2.2.2 Interpolation

We now explain how we determine the value of the auxiliary unknowns from the main unknowns (mean values of u on the grids). The solution proposed in [Yuan and Sheng, 2008] consists in finding three cell centers such that the position of the auxiliary vertex is within the convex hull of these three centers. Apart from introducing an arbitrary (several combinations of three centers may be suitable), this induces a loss of locality of the algorithm which makes it almost impossible to parallelize (on a very distorted mesh, these three centers may be at a very large topological distance from the point considered - see Figure 2.3). We take P, one of the vertices of the mesh, and consider the neighboring cells $(K_i)_{1\leq i\leq p}$, that is, all the cells containing the vertex P. We then write u_P as a linear function of the unknowns u_{K_i}:

$$u_P = \sum_{i=1}^{p} \omega_i u_{K_i}. \tag{2.13}$$

We have therefore chosen the following interpolation method. Take P, one of the vertices of the mesh, and consider the neighboring cells $(K_i)_{1\leq i\leq p}$, that is, all the cells containing the vertex P. We then write a linear approximation of u_P as a function of the unknowns u_{K_i}:

$$\left\{\begin{array}{rcl} \displaystyle\sum_{i=1}^{p} \omega_i & = & 1, \\ \displaystyle\sum_{i=1}^{p} \omega_i x_{K_i} & = & x_P, \\ \displaystyle\sum_{i=1}^{p} \omega_i y_{K_i} & = & y_P. \end{array}\right. \tag{2.14}$$

In this system, the unknowns are the weights ω_i, and (x_M, y_M) are the coordinates of the point M. It is a system of three equations and p unknowns. In most cases, $p \neq 3$. Therefore a least squares resolution is performed. In general, $p \geq 3$ (e.g. for a structured mesh of quadrangles, $p = 4$ for the vertices inside the mesh), and the system is undetermined.

This method is satisfactory in the case of diffusion coefficients κ varying only slightly in space. If the variations of κ are important, we can see that the results are clearly improved by using the space variable reduced by the opacity $X = \dfrac{x}{\kappa}, Y = \dfrac{y}{\kappa}$. The system (2.14) then becomes

$$\left\{\begin{array}{rcl} \displaystyle\sum_{i=1}^{p} \omega_i \overline{\sigma}_P & = & \overline{\sigma}_P, \\ \displaystyle\sum_{i=1}^{p} \omega_i (X_{K_i} - X_P) & = & 0, \\ \displaystyle\sum_{i=1}^{p} \omega_i (Y_{K_i} - Y_P) & = & 0. \end{array}\right. \tag{2.15}$$

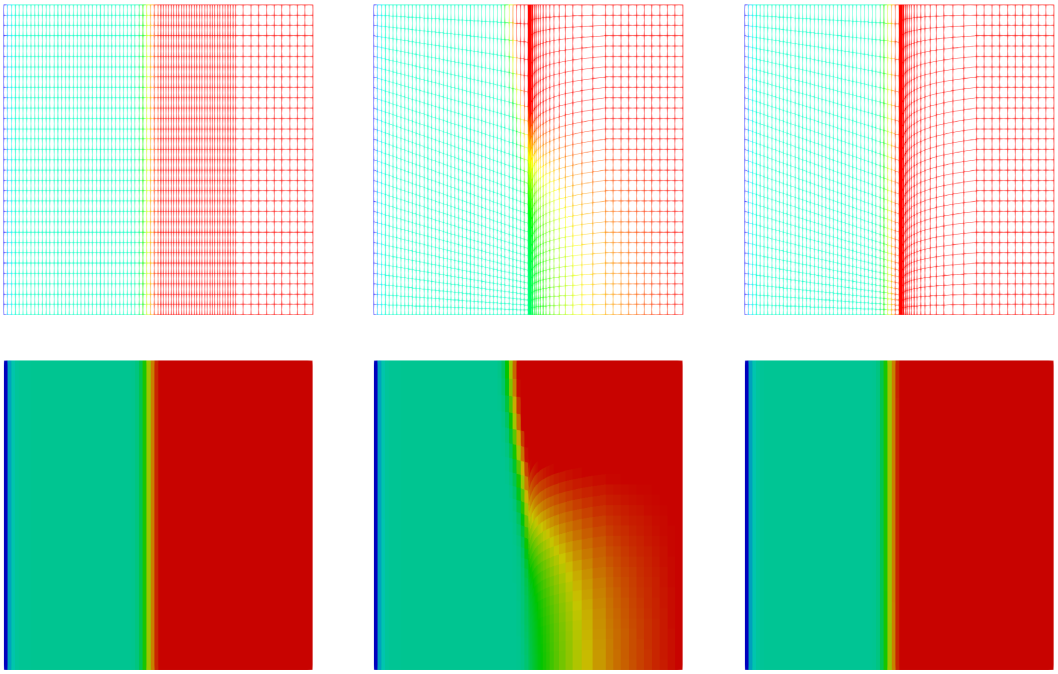

Figure 2.4: Testing the interpolation method. A transparent material (right half of the computational domain), is initially at equilibrium with an opaque material (left half). A Dirichlet condition is imposed on the right boundary, which generates a Marshak wave propagating to the left. When the wave enters the opaque material, it is deformed when the mesh is distorted and that the formula (2.14) is used (middle figures). The formula (2.15) allows to find the flatness of the wave (figures on the left). Top: mesh (color u), bottom color map of u. Left: rectangular cells, center: deformed cells, and formula (2.14), right: deformed cells and formula (2.15).

where $\overline{\sigma}_P = \sum_{i=1}^{p} \frac{1}{\kappa_i}$ is the average of the opacities and is used to size the first equation. This means that in interpolation, the cells belonging to the media with the greatest optical depth are preferred. The effect of this modification is illustrated in figure 2.4 in the case of the propagation of a Marshak wave on a deformed mesh.

Recall that one of the sufficient conditions for the solution of the previous scheme to be well defined is that $u_P \geq 0$. One way to ensure this is that all weights are positive. This is always the case if P is in the convex hull of the K_i points. This condition can be violated if the mesh is very distorted (see Figure 2.3). This difficulty can be overcome by enlarging the stencil for interpolation. However, like the method proposed by Sheng and Yuan [Yuan and Sheng, 2008], this makes parallelization of the scheme very difficult. To avoid this pitfall, the following two strategies have been put in place:

- The first one consists in projecting P on the convex hull defined by the vertices K_i. This projected Q is then used in the system (2.14) or (2.15) instead of P. This gives weights $\omega_i \geq 0$ for any i, so that $u_P \geq 0$. However, this decreases the precision of the scheme, especially if Q is far from P.

- Another possibility is to solve (2.14) or (2.15), and calculate u_P as before, but truncating the result as follows:

$$u_P = \max\left(0, \sum_{i=1}^{P} \omega_i u_{K_i}\right).$$

  This necessarily implies $u_P \geq 0$, and it doesn't affect the accuracy, since we know that, *a posteriori*, $u_P \geq 0$. Moreover, unlike the usual truncations, the scheme remains conservative.

2.2.3 Fix point iterations

As μ_1 and μ_2 depend on u, the scheme presented here is non-linear. It is thus necessary to implement an iterative algorithm to solve the discrete problem. The simplest that can be envisaged is the following:

$$\left\{ \begin{array}{l} v^0 = u^n, \\ \forall k \geq 0, \quad M(v^k)v^{k+1} = f + g, \end{array} \right. \tag{2.16}$$

with a stop criterion $\|v^{k+1} - v^k\| \leq \varepsilon \|v^k\|$. We then consider the value of u^{n+1} to be v^{k+1}.

If the problem to be solved is linear (e.g. actually (2.1)), the iterative strategy described above induces a significant over cost in calculation time (it must be solved k times the problem). However, most models of interest are in practice non-linear. Therefore, the problem (2.1) is only one step to solve a more complex model. This resolution also requires an iterative algorithm (Newton's method, by example). In fact, we solve the non-linearities induced by the scheme and by the model together. With this strategy, the cost of calculation induced by the non-linearity of the scheme is very low.

2.3 Summary

In the article [Blanc and Labourasse, 2016], we prove that the scheme:

- is conservative,
- is **positive**,
- admit a unique solution (well posed),
- is associated with a non-linear problem that converges under parabolic constraint on the time step. This constraint is strong but not necessary (just sufficient). It is thus not imposed in practice, but this property guarantees that in case of non-convergence, a decrease of the time step will solve the problem.

The demonstration of these properties (except for conservation) requires that the source term, initial conditions and boundary conditions of the problem under consideration are positive.

How would we express in terms of the statistical theory the marvellous faculty of a living organism, by which it delays the decay into thermodynamical equilibrium (death)? ... It feeds upon negative ***entropy*** *... Thus the device by which an organism maintains itself stationary at a fairly high level of orderliness (= fairly low level of* ***entropy****) really consists in continually sucking orderliness from its environment.*

Erwin Schrödinger

3 Multi-fluid hydrodynamics

Contents

3.1 Introduction

This part is dedicated to the work I have done specifically on multi-fluid issues. The mobile mesh methods described in the chapter 1 allow to describe with great precision multi-material flows. Indeed, the Lagrangian point of view allows by construction to follow contact discontinuities. This greatly facilitates the management of thermodynamic closures (equations of state) and inter-material surface terms (surface tension, friction, ...). In Section 3.3 we show how to take advantage of this feature, using surface tension forces as an example. However, these methods are fragile, as the mesh deforms with the material. Therefore, they cannot capture vortices or high shears. In the case of high shear between two fluids, methods have been developed [Clair et al., 2014, Bertoluzza et al., 2016]. They make it possible to preserve the Lagrangian viewpoint, by allowing the mesh of fluids to slide over each other. These methods are described in Section 3.5. These techniques expand the Lagrangian representation of the flow, but prove insufficient in the case of strong deformations of the contact discontinuity. In this case, the interface can no longer be captured by the mesh. An original method for maintaining an accurate representation is explained in Section 3.4. Finally, in Section 3.6, we show how to deal with the interpenetration of fluids of different velocities in the context of hot plasmas. Before that, we recall the numerical scheme used to solve the projection phase.

3.2 Projection phase

As recalled in the introduction, the algorithms used to solve the Rosseland hydrodynamics system have three phases: a hydrodynamics phase with fixed radiative entropy described in chapter 1, a

radiative wave propagation phase with fixed hydrodynamics described in chapter 2, and the phase of projection on a regularized mesh that I describe here. Between phases II and III, the mesh was regularized in order to avoid too large deformations of its elements. This step is not discussed in this manuscript and the interested reader may refer to [Winslow, 1966, Knupp, 2000b,c, Escobar et al., 2003]. This last part of the resolution thus consists only in representing the solution obtained at the end of phases I and II on this new mesh, ideally without alteration. This is impossible. However, in order to maintain the coherence of the whole resolution, constraints of consistency, conservation, and stability are imposed during this phase. The principles of the method used, known as *swept*, are described in [Benson, 1992c]. It consists in representing the problem of projection of the Lagrangian mesh on the regularized mesh by the following system, obtained by application of Reynolds' theorem

$$\frac{d}{dt}\int_j 1 - \int_j \nabla\cdot\mathbf{w} = 0, \tag{3.1}$$

$$\frac{d}{dt}\int_j \rho - \int_j \nabla\cdot\rho\mathbf{w} = 0, \tag{3.2}$$

$$\frac{d}{dt}\int_j \rho\mathbf{u} - \int_j \nabla\cdot\rho\mathbf{w}\otimes\mathbf{u} = \mathbf{0}, \tag{3.3}$$

$$\frac{d}{dt}\int_j \rho E - \int_j \nabla\cdot\rho\mathbf{w}E = 0. \tag{3.4}$$

on any cell Ω_j. By integrating the previous system in time, and using Green's formula, we obtain

$$\int_t^{t+\Delta t}\frac{d}{dt}\int_j \varphi - \int_t^{t+\Delta t}\int_{\partial j}\varphi\mathbf{w}\cdot\mathbf{n} = 0, \tag{3.5}$$

where φ is 1, ρ, $\rho\mathbf{u}$ or ρE. In this equation, the velocity $\mathbf{w}$ and the time step Δt can be chosen arbitrarily as long as they respect for each vertex of the mesh the constraint

$$\int_t^{t+\Delta t}\mathbf{w}_r = \mathbf{x^R}_r - \mathbf{x^L}_r, \tag{3.6}$$

where $\mathbf{x^R}_r$ and $\mathbf{x^L}_r$ are respectively the rezoned position and the position at the end of the Lagrangian phase of the vertex r. Considering that this step transforms a polyhedral (resp. polygonal) mesh into another polyhedral (resp. polygonal) mesh, one can choose for convenience $\mathbf{w}$ affine on each edge of the elements and constant in time, and the previous system can be rewritten without approximation

$$|\Omega_j|^R\varphi_j^R - |\Omega_j|^L\varphi_j^L = -\sum_{e\sim j}\mathbf{w}_e\cdot\int_t^{t+\Delta t}\int_e\varphi\mathbf{n}, \tag{3.7}$$

where e refers to the edges and $e\sim j$ refers to all the edges of the cell j. We can see that if we apply this formula to the function $\varphi = 1$, the right-hand-side corresponds to the algebraic volume $\delta\Omega_e$ shown in Figure 3.1. An exact formula for the volume conservation equation is deduced from it

$$|\Omega_j|^R - |\Omega_j|^L = \sum_{e\sim j}\delta\Omega_e. \tag{3.8}$$

In a similar way, the fluxes of $\varphi = \rho$, $\rho\mathbf{u}$ or ρE

$$\varphi_j^R|\Omega_j|^R - \varphi_j^L|\Omega_j|^L = \sum_{e\sim j}\varphi_e\delta\Omega_e. \tag{3.9}$$

At order 1, we choose φ_e according to the sign of $\delta\Omega_e$, so as to ensure stability. The upwind scheme is written

$$\varphi_e = \begin{cases}\varphi_j^L & \text{if } \delta\Omega_e > 0,\\ \varphi_{j'}^L & \text{else,}\end{cases} \tag{3.10}$$

with the notations of the figure 3.1. The first-order version of this algorithm respects the maximum principle on ρ, $\mathbf{u}$ (in the sense of the convex hull [Hoch and Labourasse, 2014]) and E. As in the scheme for the Lagrangian phase, this method is extended to order 2 by a MUSCL procedure. The maximum principle is ensured by the joint use of a Barth Jespersen [Barth and Jespersen, 1989b] limiter and the Apitali method described in Section 1.6.2.

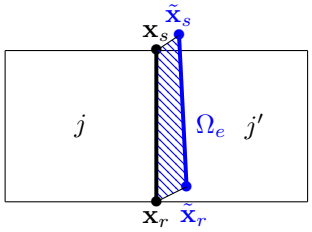

Figure 3.1: Swept method

3.3 Application to surface tension

In collaboration with T. Corot, and P. Hoch

I describe in this section the insertion of surface tension forces in the Lagrangian scheme described in chapter 1. The type of application aimed at is the study of the particle distribution induced by the impact of a shock on the disturbed surface of a fluid (Richtmyer-Meshkov instability). The simulation of this phenomenon requires the ability to take into account, in a precise and robust way, strong shocks and surface tension. Although quite a lot of work has been devoted to modelling and simulating surface tension over the last few decades, it has mainly focused on incompressible or low Mach number flows. Only a few recent works deal with compressible flows [Chang et al., 2013, Fechter et al., 2018, Fuster and Popinet, 2018, Garrick et al., 2017, Nguyen and Dumbser, 2015, Perigaud and Saurel, 2005, Rohde and Zeiler, 2015, Chauveheid, 2015, Schmidmayer et al., 2017]. Our approach is original because it is based on the ALE formalism described above. The objective is to maintain as long as possible the interface between the fluids Lagrangian, in order to take advantage of the accuracy of the Lagrangian description. Then, when the interface is too distorted, the mesh is regularized, and the interfaces are followed with a VOF (Volume Of Fluid) methodology. This requires a method capable of handling unstructured meshes, which is also quite rare.

We consider two fluids in d dimension separated by an interface. Each fluid is characterized by its density ρ_k and its internal energy e_k, with $k \in \{0, 1\}$. The Σ interface of dimension $d-1$ is implicitly defined by a function at least $\mathcal{C}^2$, $f(\mathbf{x}, t) = 0$, $\mathbf{x} \in \mathbb{R}^d$. We assume that $\nabla f(\mathbf{x}, t) \neq \mathbf{0}$, at least for $(\mathbf{x}, t)$ s.t. $f(\mathbf{x}, t) = 0$. We can then set the normal vector to Σ by $\mathbf{n} = \frac{\nabla f}{|\nabla f|}$ for all $(\mathbf{x}, t)$ s.t. $f(\mathbf{x}, t) = 0$ (see for instance [Goldman, 2005]).Note $\delta_\Sigma = \delta(f(\mathbf{x}, t))$ the Dirac distribution associated with Σ. We further assume that there is no mass transfer through Σ. The surface tension terms modify the system (14)-(17) by adding a non-conservative, surface tension term to the momentum and energy balance equations. The system corresponding to phase I is then written in continuous form and in the sense of the distributions [Kataoka, 1986]

$$\begin{aligned}
&\frac{\partial}{\partial t}\rho + \nabla \cdot (\rho \mathbf{u}) = 0, \\
&\frac{\partial}{\partial t}(\rho \mathbf{u}) + \nabla \cdot (\rho \mathbf{u} \otimes \mathbf{u}) + \nabla p_T = \sigma \kappa \mathbf{n} \delta_\Sigma, \\
&\frac{\partial}{\partial t}(\rho E) + \nabla \cdot (\rho \mathbf{u} E) + \nabla \cdot (p_T \mathbf{u}) = \sigma \kappa \mathbf{n} \cdot \mathbf{u} \delta_\Sigma.
\end{aligned} \tag{3.11}$$

In [Corot et al., 2020], we propose an extension of the Lagrangian scheme presented in the first part to solve this system of equations. This scheme is well-balanced in the sense that it exactly preserves the Laplace's law which characterizes the pressure jump across the interface as a function of the curvature κ. The positivity of the density, temperature and entropy growth of the two fluids is also assured. We describe how to take into account the remeshing of the interface when it becomes inevitable. An example of illustration of this method is proposed in figure 3.2.

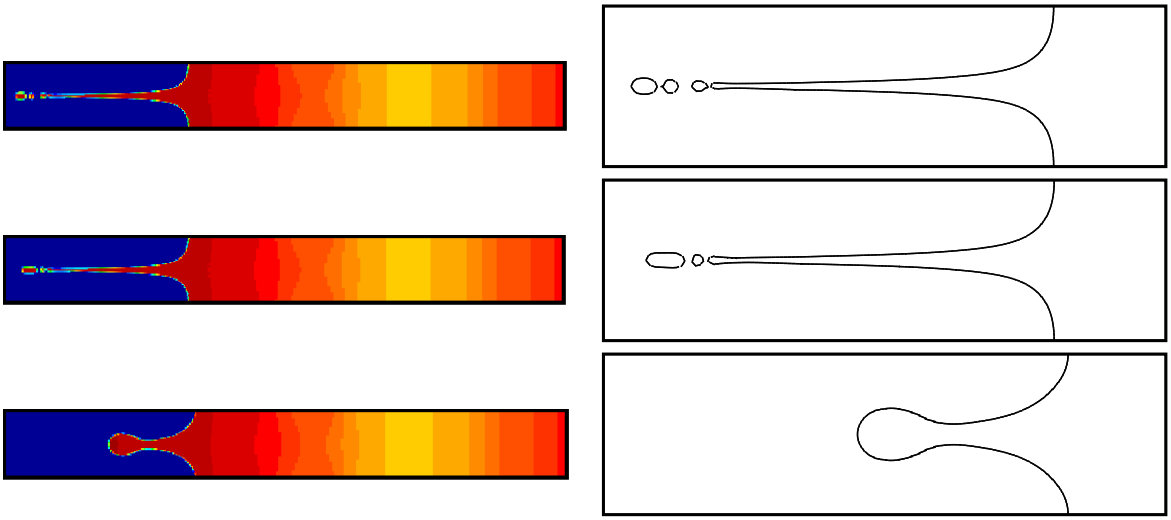

Figure 3.2: Richtmyer-Meshkov instability. Density maps (left) and interface (right) for a surface tension coefficient σ =0 (top figure), $\sigma = 0.0001$ (middle figure) and $\sigma = 0.005$ (bottom figure).

3.4 Anti-diffusive fluxes for interface preservation

In collaboration with B. Després, F. Lagoutière et I. Marmajou

We are interested here in the case where the interface between two fluids is too deformed to be able to remain coincident with a mesh line, which happens almost systematically for truly multi-dimensional flows. The interface is then immersed in the mesh, like traditional Eulerian methods. By nature, phase I (Lagrangian) does not *spread* this interface. On the other hand, phase III of the algorithm (projection on the regularized mesh), induces a numerical bias which can be dramatic for the precision of the calculations. We show (in 1D) that the truncation error of a first-order advection scheme is a diffusion term whose coefficient is proportional to the sum of the time step and the space step. This means that the numerical mixing zone (the place where fluids are mixed) grows spatially as $\sqrt{t}$. This induces a dramatic loss of precision, or even the impossibility to process certain phenomena (surface forces, chemical reactions, ...). It is therefore crucial to have a mechanism to prevent this numerical diffusion of the interface. In the Eulerian community, there are four families of methods to deal with this problem: front-tracking methods [Tryggvason et al., 2001, Unverdi and Tryggvason, 1992], Ghost-Fluid [Fedkiw et al., 1999], level-set [Osher et al., 2004] and Volume of Fluid (VoF) [Hirt and Nichols, 1981]. These methods suffer either from a lack of robustness (front-tracking), or from conservation flaws (level-set), or from a high calculation cost and complex management as soon as the number of fluids is > 2 (Ghost-Fluid, VoF). This is why we propose an interface preservation algorithm based on anti-diffusion fluxes [Després et al., 2010]. This is a multi-dimensional generalization of the algorithm proposed in [Jaouen and Lagoutière, 2007]. It allows to process an arbitrary number of fluids while keeping the partial concentrations of the constituents between 0 and 1 and the global constraints that the sum of the concentrations is equal to 1. The generalization to 3D of this method called VoFiRe (Volume Finite with Reconstruction) is immediate, and its parallelization by domain decomposition is easy.

3.5 Numerical methods for the sliding

(En collaboration avec S. Bertoluzza, G. Clair, S. Del Pino et B. Després)

The perfect sliding of two fluids over each other along an interface is a purely numerical problem. Indeed, Euler's equations contain the solutions sliding along contact discontinuities, since there is no molecular viscosity.

In Eulerian formulation, if the sliding line is a straight line of the mesh, most numerical methods allow to keep the contact discontinuity, especially for the tangential velocity. In Lagrangian formula-

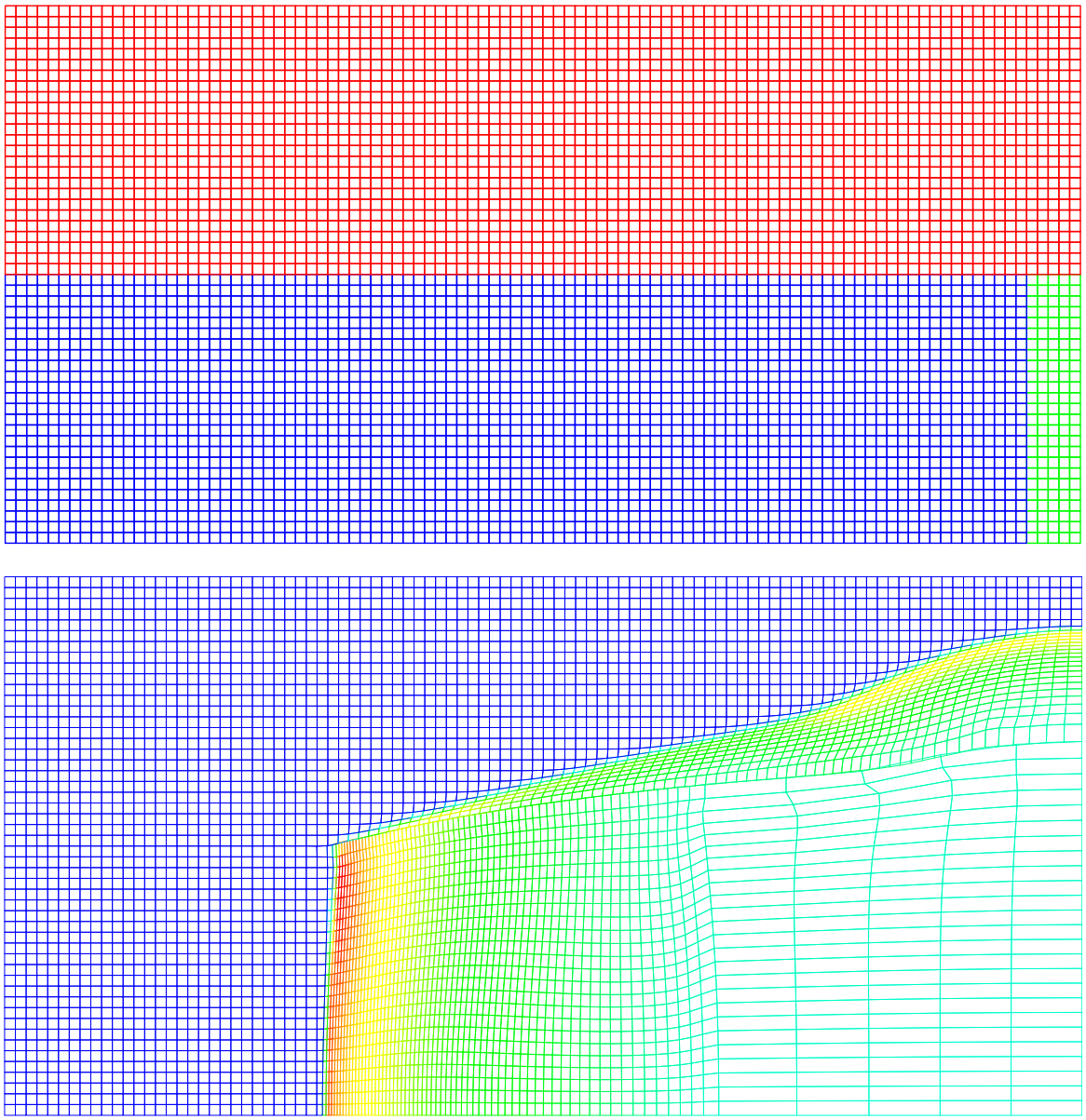

Figure 3.3: Sliding example (see [Caramana, 2009]). The material corresponding to the upper part of the mesh is heavy ($\rho = 10$), the other light ($\rho = 1$). An initial over-pressure is imposed in the green part giving rise to the sliding. *Top* : the initial configuration composed of 2 meshes (in red and green/blue). *Bottom* : the sliding of the meshes and the pressure field at time 0.3.

tion, since the mesh speed is continuous, the sliding can only be obtained at convergence. Moreover, as the smaller the cells are, the faster they will be sheared, it is illusory to try to calculate this type of flow by refining : either the mesh quickly becomes invalid, or the time step collapses. It is therefore necessary, in a way, to uncouple the mesh to allow discontinuities in the tangential velocity at the interface. This approach is often used when sliding (perfect or not) from one solid to another or from a fluid to a solid. To do this, each of the sliding constituents is associated with its own mesh, so that each block has its own speed. The pieces are then "glued" by applying non-interpenetration constraints to the different fluid domains. The literature is very extensive in this field (see for example the journal article [Bourago and Kukudzhanov, 2005]). Concerning Lagrangian methods, recent results are presented in [Caramana, 2009, Kucharick et al., 2012]. In this work, although the underlying hydrodynamic scheme [Caramana et al., 1998b] is conservative, the total energy is not conserved in the cells adjacent to the slide line. The lack of conservation is even used there as an indicator *a posteriori* of the quality of the solution.

We have proposed two different approaches to achieve a conservative (in mass, impulse and total energy) treatment of the sliding. We briefly describe here the ideas of these methods that we published in [Clair et al., 2014, Bertoluzza et al., 2016].

Both methods are based on the same construction principle and differ on the application of this principle. In both cases, we write **separately** the discrete Euler equations for every single fluid. The calculation of the fluxes is then reformulated under the form of a minimization problem for the auxiliary unknown corresponding to the volume flux ($\mathbf{u}_r$ in the classic formulation of centered schemes, see Section 1.2). A constraint of non-interpenetration (linear) of one fluid in the other one is imposed on this unknown at the common boundary of the two fluids. We then obtain a linear stress minimization problem. This stress minimization problem is solved in a weak way. The two approaches differ in the formulation of this problem.

3.5.1 First approach

In this first approach, the minimization problem to be solved is equivalent to the Riemann solver presented in Section 1.2). It consists in solving at each vertex of the mesh

$$\mathbf{u}_r = \underset{\mathbf{v}\in\mathbb{R}^d}{\operatorname{argmin}} \left(\frac{1}{2} {}^t\mathbf{v} \cdot A_r \mathbf{v} - \sum_{j\in\mathcal{J}_r} \left({}^t\mathbf{v} A_{jr} \mathbf{u}_j + \mathbf{C}_{jr} p_j \cdot \mathbf{v} \right) \right),$$

yielding the momentum flux

$$\mathbf{F}_{jr} = \mathbf{C}_j p_j + A_{jr} \left(\mathbf{u}_j - \mathbf{u}_r \right).$$

This minimization problem at each vertex of a mesh can be written in a global way by defining $\mathbf{V} := (\mathbf{v}_1, \mathbf{v}_2, ..., \mathbf{v}_N) \in \mathbb{R}^{N\times d}$, $J(\mathbf{V}) := \sum_r J_r(\mathbf{v}_r)$, and $\mathbf{U} := \underset{\mathbf{V}\in\mathbb{R}^{N\times d}}{\operatorname{argmin}} J(\mathbf{V})$, where N is the number of vertices of the mesh. A functional of this type is defined for each of the fluids on either side of the sliding line. The two problems are then decoupled.

The heart of the algorithm lies in the application of the constraint. The difficulty (illustrated in figure 3.4) is that the discrete sliding lines are different for the two computational domains. In this approach, the choice is made to duplicate the vertices of this line from one mesh to the other, as shown in the figure 3.4. For each fictitious vertex facing one of the two meshes, a velocity is computed using the tools developed in the article [Claisse et al., 2012], and recalled in Section 1.8. The constraint then consists in imposing that the normal jump of the velocity of this fictitious vertex with respect to the velocity of the real vertex, is null. The global problem of minimization under constraints is then solved in using the techniques described in the article [Clair et al., 2013].

3.5.2 Second approach

In this second approach [Bertoluzza et al., 2016], starting from the continuous formulation given in [Del Pino, 2010], one writes **separately** the problems related to the calculations of the velocities of the two grids. We then have two problems of the form, $\forall i \in \{1, 2\}$, find $\mathbf{u}_i^\star \in \mathbb{V}_i$ such that

$$\forall \mathbf{v}_i \in \mathbb{V}_i, \quad a_i(\mathbf{u}_i^\star, \mathbf{v}_i) = l_i(\mathbf{v}_i), \tag{3.12}$$

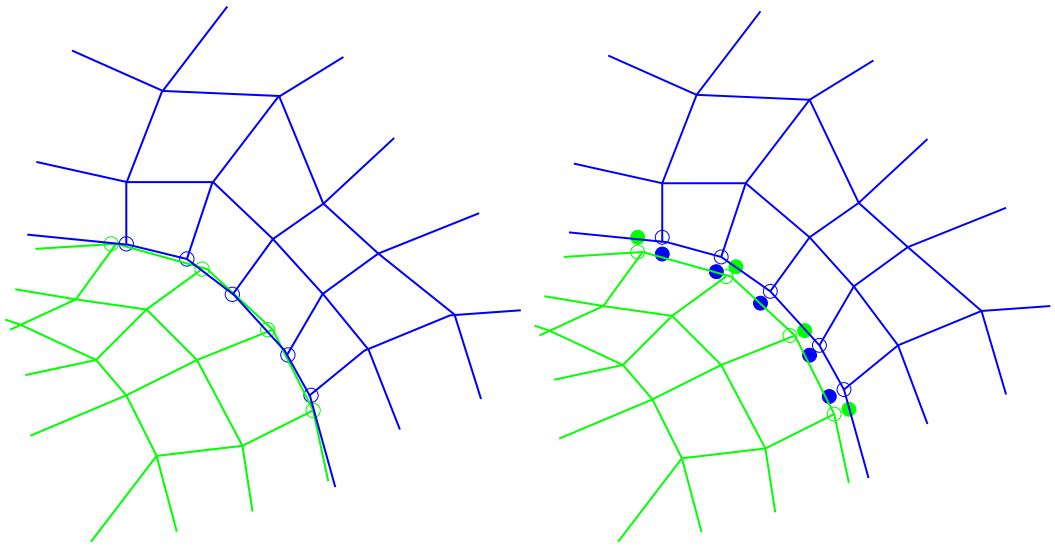

Figure 3.4: The discrete slide line does not coincide in the two calculation domains. A fictitious line, corresponding to the union of the vertices of the two lines is reconstructed, and the vertices of this line are duplicated from one mesh to the other (first approach).

where a_i are continuous bilinear forms and l_i are continuous linear forms that allow to describe grid velocities in independent ways. If the approximation spaces $\mathbb{V}_i$ are chosen so that the grid velocities are continuous and affine on each edge, then the forms a_i are coercive. The two independent problems are thus well posed: the velocities $\mathbf{u}_i^\star$ of the two grids are determined in a unique way.

The problem of perfect sliding can therefore be addressed by choosing a pair of spaces $(\mathbb{V}_1, \mathbb{V}_2)$ which ensures the continuity of the normal component on the sliding line, but this is difficult in practice.

On the other hand, the properties of the forms a_i and l_i allow to reformulate variational problems as minimization problems. If we define

$$\begin{aligned} \forall i \in \{1,2\}, \quad J_i : \mathbb{V}_i &\mapsto \mathbb{R}, \\ \mathbf{v}_i &\to J_i(\mathbf{v}_i) := \tfrac{1}{2} a_i(\mathbf{v}_i, \mathbf{v}_i) - l_i(\mathbf{v}_i), \end{aligned}$$

then $\forall i \in \{1,2\}$, the solution $\mathbf{u}_i^\star$ of (3.12) verifies

$$\forall \mathbf{v}_i \in \mathbb{V}_i, \qquad J_i(\mathbf{u}_i^\star) \leq J_i(\mathbf{v}_i).$$

It is then natural to look for the solution of the sliding problem as a solution of the minimization problem in $\mathbb{V}_1 \times \mathbb{V}_1$ of $J_1(\mathbf{v}_1) + J_2(\mathbf{v}_2)$, under the constraint of perfect sliding

$$\forall \mu \in \mathbb{L}, \quad \int_\Gamma (\mathbf{u}_1^\star - \mathbf{u}_2^\star) \cdot \mathbf{n} \mu = 0,$$

where $\mathbb{L}$ is a test function space that we won't describe here and $\mathbf{n}$ is the unitary normal at the sliding interface Γ between the two meshes. This constrained problem can be expressed using Lagrange multipliers in the form

Find $(\mathbf{u}_1^\star, \mathbf{u}_2^\star, \lambda) \in \mathbb{V}_1 \times \mathbb{V}_2 \times \mathbb{L}$ so that

$$\begin{aligned} \forall (\mathbf{v}_1, \mathbf{v}_2, \mu) \in \mathbb{V}_1 \times \mathbb{V}_2 \times \mathbb{L}, \qquad & \sum_{i \in \{1,2\}} a_i(\mathbf{u}_i^\star, \mathbf{v}_i) + \sum_{i \in \{1,2\}} b_i(\mathbf{v}_i, \lambda) = \sum_{i \in \{1,2\}} l_i(\mathbf{v}_i), \\ & \text{and} \quad \sum_{i \in \{1,2\}} b_i(\mathbf{u}_i^\star, \mu) = 0, \end{aligned}$$

where $b_i(\mathbf{v}, \mu) := \int_\Gamma \mathbf{v} \cdot \mathbf{n} \mu$.

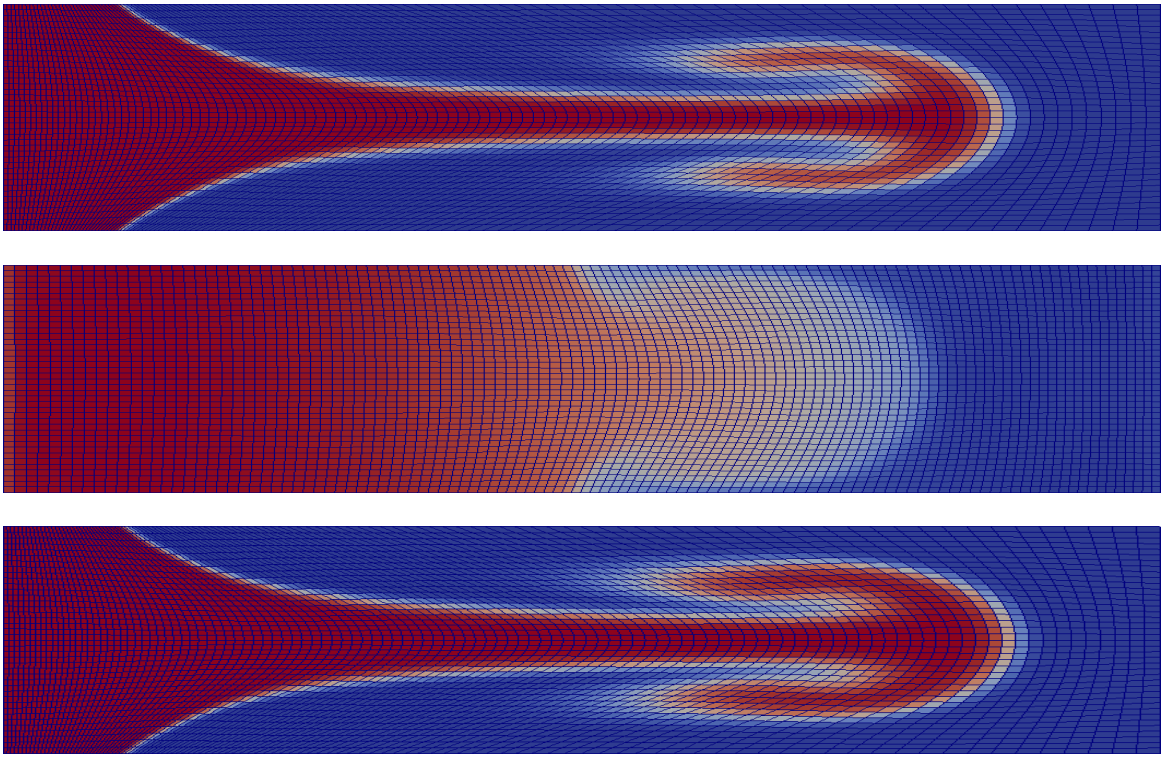

Figure 3.5: Rayleigh-Taylor instability: the upper figure corresponds to the concentration field for a single-fluid calculation used as a reference. The middle figure is obtained using a non-AP scheme and a coefficient of friction of 10^6. The lower figure is obtained using the AP scheme proposed in this document.

In [Bertoluzza et al., 2016], we have given a method describing how to mesh Γ so that the numerical method finally obtained allows the calculation of grid velocities in a unique way, while ensuring the conservation of mass, momentum and total energy. Let us note nevertheless, that in the general case, the volume is not preserved,[1] which does not allow to obtain an entropic scheme on the mesh layer at the interface.

3.6 Multi-velocity and asymptotic preserving numerical method

In collaboration with S. Del Pino and G. Morel

An original way of dealing with the interaction between fluids is to consider that they occupy the same regions of space and interact simply by terms such as friction or heat exchange.

Such **multi-fluid models** have the advantage of processing mixtures with a focus on interaction modelling. For these models, each fluid is described by its own set of variables (density, velocity and energy). A multi-fluid model popular is the Baer-Nunziato [Baer and Nunziato, 1986] model that describes the transition from deflagration to detonation for reactive fluids. This type of model is also used to describe the plasma collision or for dealing with non-local thermodynamic equilibrium [Sentis, 2014]. Scannapieco and Cheng [Scannapieco and Cheng, 2002] have developed a similar model for turbulent fluids, and have applied it to describe the evolution of a mixing zone due to Rayleigh-Taylor or Richtmyer-Meshkov type instabilities.

During G. Morel's internship, we studied a simplified version of the Scannapieco-Cheng model, where only the friction between the two fluids is considered. The framework of this study is the multidimensional ALE formalism and generalizes in a certain way the work of Enaux's thesis [Enaux,

[1] This is due to the fact that the sliding line itself is not clearly defined for two polygonal meshes sliding on each other.

2007] which used a directional splitting approach. The simplified bi-fluid model is written as follows

$$\begin{aligned}
\rho^\alpha D_t^\alpha \tau^\alpha &= \nabla \cdot \mathbf{u}^\alpha, \\
\rho^\alpha D_t^\alpha \mathbf{u}^\alpha &= -\nabla p^\alpha - \nu\rho\delta\mathbf{u}^\alpha, \\
\rho^\alpha D_t^\alpha E^\alpha &= -\nabla \cdot (p^\alpha \mathbf{u}^\alpha) - \nu\rho\delta\mathbf{u}^\alpha \cdot \bar{\mathbf{u}},
\end{aligned}$$

where $\alpha \in \{1,2\}$ is one of the two fluids and $\beta = 3-\alpha \in \{1,2\}$ is the other fluid. Each fluid α is defined by its own state : $(\rho^\alpha, \mathbf{u}^\alpha, E^\alpha)$. The operator $\delta(\cdot)^\alpha$ is defined by $\delta\phi^\alpha = -\delta\phi^\beta = \phi^\alpha - \phi^\beta$ for all quantity ϕ. One denotes $\nu \in \mathbb{R}^+$ the friction coefficient, $\rho := \rho^\alpha + \rho^\beta$ and $\rho\bar{\mathbf{u}} := \rho^\alpha\mathbf{u}^\alpha + \rho^\beta\mathbf{u}^\beta$. For each fluid, $p^\alpha := p^\alpha(\rho^\alpha, e^\alpha)$, where $e^\alpha := E^\alpha - \frac{1}{2}\|\mathbf{u}^\alpha\|^2$. Finally, note that the Lagrangian derivative $D_t^\alpha := \partial_t + \mathbf{u}^\alpha \cdot \nabla$ is different from one fluid to another.

The objective of this model is to study the behaviour of numerical methods as a function of the coefficient ν since, in the end, this coefficient can be replaced by a function of the states of the two fluids in order to better model their interaction. For these finer models, the coefficient can vary strongly, and as Sentis [Sentis, 2014] indicates *"this system can be difficult to solve in dimensions two or three, especially when the coefficient of friction is large"*. In this work, we therefore propose a numerical method that is not sensitive (in terms of precision) to values of ν.

The usual framework for parameter-dependent methods is the family of **Asymptotic Preserving (AP) schemes**. The idea of these schemes is to mimic the behavior of the model when the parameter ν tends towards infinity. Indeed, if for any consistent scheme, when ν is fixed, we know that at convergence the solution will be correct, nothing indicates which grid fineness will be sufficient to obtain an enough accurate solution. In practice, it is therefore possible that for $\nu >> 1$, this mesh fineness is out of reach even for simple flows. The idea of AP schemes is therefore to add information (usually in numerical fluxes) so that the limit scheme ($\nu \to \infty$) is *a priori* consistent with the limit model.

The proposed scheme has the property of preserving the asymptotic in addition to the classic properties of conservation, entropy and consistency. It is written in semi-discrete form, $\forall\alpha \in \{1,2\}$,

$$\begin{aligned}
m_j^\alpha d_t \tau_j^\alpha &= \sum_{r\in\mathcal{R}_j} \mathbf{C}_{jr}^\alpha \cdot \mathbf{u}_r^\alpha, \qquad d_t m_j^\alpha = 0, \\
m_j^\alpha d_t \mathbf{u}_j^\alpha &= -\sum_{r\in\mathcal{R}_j} \mathbf{F}_{jr}^\alpha - \sum_{r\in\mathcal{R}_j} \nu\rho_r B_{jr}\delta\mathbf{u}_j^\alpha, \\
m_j^\alpha d_t E_j^\alpha &= -\sum_{r\in\mathcal{R}_j} \mathbf{F}_{jr}^\alpha \cdot \mathbf{u}_r^\alpha - \sum_{r\in\mathcal{R}_j} \nu\rho_r \bar{\mathbf{u}}_r^T B_{jr}\delta\mathbf{u}_j^\alpha + \sum_{r\in\mathcal{R}_j} \nu\rho_r \bar{\mathbf{u}}_{jr}^T B_{jr}(\delta\mathbf{u}_r^\alpha - \delta\mathbf{u}_j^\alpha),
\end{aligned}$$

where the fluxes are defined by

$$\begin{aligned}
\mathbf{F}_{jr}^\alpha &= \mathbf{C}_{jr} p_j^\alpha - A_{jr}^\alpha(\mathbf{u}_r^\alpha - \mathbf{u}_j^\alpha) - \nu\rho_r B_{jr}\delta\mathbf{u}_r^\alpha, \\
\sum_{r\in\mathcal{R}_j} \mathbf{F}_{jr}^\alpha &= \mathbf{0}.
\end{aligned}$$

To write this scheme, the following notations have been introduced : ρ_r^α is the mean values in the cells j around the vertex r of ρ_j^α and $\rho_r := \rho_r^\alpha + \rho_r^\beta$. We have defined $\bar{\mathbf{u}}_r$ and $\bar{\mathbf{u}}_{jr}$ with

$$\rho_r\bar{\mathbf{u}}_r = \rho_r^\alpha\mathbf{u}_r^\alpha + \rho_r^\beta\mathbf{u}_r^\beta, \qquad \text{and} \qquad \rho_r\bar{\mathbf{u}}_{jr} = \rho_r^\alpha\mathbf{u}_j^\alpha + \rho_r^\beta\mathbf{u}_j^\beta.$$

Finally, the matrices B_{jr} are symmetric define positive such that $\sum_{r\in\mathcal{R}_j} B_{jr} = V_j I$. The other notations are classical.

On figure 3.5, we give an example comparing the effect of the AP scheme, to the solution of a consistent but more naive scheme (not integrating friction in the flow calculation).

Note that this work was published in 2018 [Del Pino et al., 2018].

In science it often happens that scientists say, 'You know that's a really good argument; my position is mistaken,' and then they would actually change their minds and you never hear that old view from them again. They really do it. It doesn't happen as often as it should, because scientists are human and change is sometimes painful. But it happens every day. I cannot recall the last time something like that happened in politics or religion.

Carl Sagan

Conclusion and prospects

In this thesis, I described my work at CEA DAM. During these 15 years, I have proposed numerical methods to solve different models in the framework of radiative compressible hydrodynamics. The problems addressed in this manuscript are extensive and deal with the resolution of parabolic and hyperbolic systems. The common points of this work are the observation of fundamental principles, which have guided it: consistency with the system of equations to be solved, respect of conservation laws, and stability (in the sense non-linear stability and respect of the mathematical or physical constraints of the systems of equations). Once these specifications were met, I focused on ensuring other important properties of the systems of equations under consideration, such as Galilean invariance, respect of equilibrium or asymptotic limits.

The continuation of this work is already under way and is based on two axes: the enhancement of the order of approximation and the extension of the model.

The very high-order extension for Lagrangian hydrodynamics has already been the subject of a publication [Carré et al., 2009b], relating to high-order fluxes. The main difficulty that remains to be solved is related to geometry. Indeed, in the Lagrangian context, compliance with the geometric conservation law implies that a method based on polygonal or polyhedral meshes is of order 2 at the most. It is therefore essential to enrich the geometry of the cells in order to be able to envisage an order of approximation higher than 2. Recent work based on Discontinuous Galerkin's method [Vilar, 2012, Vilar et al., 2014, Liu et al., 2018a,b] shows the feasibility of this. However, the capture of strong shocks by Discontinuous Galerkin methods remains a major difficulty. This is why, with Stéphane Del Pino and Philippe Hoch, we propose an original method inspired by [Del Pino, 2011]. It is a finite volume scheme which can be seen as a generalization of the schemes presented in chapter 1. The fluxes are reconstructed on curvilinear edges by a finite element method. We are able to prove the weak consistency of the resulting schemes family, under the assumption that the solution is in BV^2. This study is the subject of a paper in preparation [Del Pino et al., 2020b]. However, many points remain to be explored in order to make an industrial use of this type of schemes. Work on the high-order extension of the diffusion operator is less advanced. For the reasons recalled in chapter 2, we are moving towards a finite volume method. One of the challenges will be to respect the positivity constraint of the unknown, as for the scheme described in chapter 2.

The extension of hydrodynamics to the Navier-Stokes model has already been the subject of a M2 internship in 1D [Chopot, 2016]. We are continuing this study, in order to propose a multi-dimensional scheme respecting the above-mentioned principles. For the radiation part, we study transport models (P1, M1, Sn, see for example [Castor, 2004] for a hierarchy of these models), in order to widen the field of applications to less opaque media. An internship has already been carried out on the P1 model coupled with matter [Rambaud, 2016]. We are now exploring a Sn modeling based on a macro-micro [Crouseilles and Lemou, 2011] splitting. These methods have the advantage of capturing by construction the diffusion limit of the transport equations, which is a fundamental objective in our applications.

[2] bounded variation functions

References

Author's journal articles cited in this document

S. Bertoluzza, S. Del Pino, and E. Labourasse. A conservative slide line method for cell-centered semi-Lagrangian and ALE schemes in 2D. *ESAIM: Math. Model. Numer. Anal.*, 50(1):187–214, 2016.

X. Blanc and E. Labourasse. A positive scheme for diffusion problems on deformed meshes. *J. Appl. Math. Mech.*, 96(6):660–680, 2016.

G. Carré, S. Del Pino, B. Després, and E. Labourasse. A cell-centered Lagrangian hydrodynamics scheme in arbitrary dimension. *J. Comput. Phys.*, 228(14):5160–5183, 2009a.

G. Carré, S. Del Pino, E. Labourasse, K. Pichon Gostaf, and A. V. Shapeev. Polynomial Least-Square reconstruction for semi-Lagrangian Cell-Centered Hydrodynamic Scheme. *ESAIM: Proc.*, 4(5):1008–1024, November 2009b.

G. Clair, B. Després, and E. Labourasse. A new method to introduce constraints in cell-centered Lagrangian schemes. *Comp. Meth. Appl. Mech. Eng.*, 261:56–65, 2013.

G. Clair, B. Després, and E. Labourasse. A one-mesh method for the cell-centered discretization of sliding. *Comp. Meth. Appl. Mech. Eng.*, 269:315–333, 2014.

A. Claisse, B. Després, E. Labourasse, and F. Ledoux. A new exceptional points method with application to cell-centered Lagrangian schemes and curved meshes. *J. Comput. Phys.*, 231:4324–4354, 2012.

T. Corot, P. Hoch, and E. Labourasse. Surface tension for compressible fluids in ALE framework. *J. Comput. Phys.*, 407:109247, 2020.

S. Del Pino, E. Labourasse, and G. Morel. An asymptotic preserving multidimensional ALE method for a system of two compressible flows coupled with friction. *J. Comput. Phys.*, 363:268 – 301, 2018.

S. Del Pino, P. Hoch, and E. Labourasse. Frame invariant and entropic second-order cell-centered ALE schemes. in preparation, 2020a.

S. Del Pino, P. Hoch, and E. Labourasse. Arbitrary high-order semi-Lagrangian finite volume schemes for gas dynamics. in preparation, 2020b.

B. Després and E. Labourasse. Stabilization of cell-centered compressible Lagrangian methods using subzonal entropy. *J. Comput. Phys.*, 231(20):6559 – 6595, 2012.

B. Després and E. Labourasse. Angular momentum preserving cell-centered Lagrangian and Eulerian schemes on arbitrary grids. *J. Comput. Phys.*, 290:28–54, 2015.

B. Després, F. Lagoutière, E. Labourasse, and I. Marmajou. An antidissipative transport scheme on unstructured meshes for multicomponent flows. *Int. J. Finite Volumes*, 7:30–65, 2010.

P. Hoch and E. Labourasse. A frame invariant and maximum principle enforcing second-order extension for cell-centered ALE schemes based on local convex hull preservation. *Int. J. Numer. Meth. Fluids*, 76:1043–1063, 2014.

E. Labourasse. A low-Mach correction for multi-dimensional finite volume shock capturing schemes with application in Lagrangian frame. *Comput. Fluids*, 179:372 – 393, 2019.

Lectures by the author, cited in this document

P. Hoch and E. Labourasse. Entropic and Galilean invariant second-order extension for cell-centered Lagrangian schemes. In *ECCOMAS*, Barcelona, July 2014.

Other journal articles by the author

E. Labourasse and P. Sagaut. Reconstruction of Turbulent Fluctuations Using a Hybrid RANS/LES Approach. *J. Comput. Phys.*, 182(1):301 – 336, 2002.

E. Labourasse and P. Sagaut. Advance in RANS-LES coupling, a review and an insight on the NLDE approach. *Arch. Comput. Methods Eng.*, 11(3):199–256, 2004.

E. Labourasse, D. Lacanette, A. Toutant, P. Lubin, S. Vincent, O. Lebaigue, J.-P. Caltagirone, and P. Sagaut. Towards Large Eddy simulation of isothermal two-phase flows: Governing equations and a priori tests. *Int. J. Multiphase Flow*, 33(1):1 – 39, 2007.

P. Sagaut, E. Labourasse, P. Quéméré, and M. Terracol. Multiscale approaches to unsteady simulation of turbulent flows. *Int. J. Nonlin. Sci. Num.*, 1(4):285–298, 2000.

P. Sagaut, E. Garnier, E. Tromeur, L. Larcheveque, and E. Labourasse. Turbulent inflow conditions for Large-Eddy-Simulation of compressible wall-bounded flows. *AIAA J.*, 42(3):469 – 477, 2004a.

P. Sagaut, E. Garnier, E. Tromeur, L. Larcheveque, and E. Labourasse. Special section: boundary conditions for Large Eddy Simulation-Turbulent Inflow Conditions for Large-Eddy Simulation of Compressible Wall-Bounded Flows. *AIAA J.*, 42(3):469–477, 2004b.

M. Terracol, E. Manoha, C. Herrero, E. Labourasse, S. Redonnet, and P. Sagaut. Hybrid methods for airframe noise numerical prediction. *Theor. Comput. Fluid Dyn.*, 19(3):197–227, 2005.

A. Toutant, E. Labourasse, O. Lebaigue, and O. Simonin. DNS of the interaction between a deformable buoyant bubble and a spatially decaying turbulence: A priori tests for LES two-phase flow modelling. *Comput. Fluids*, 37(7):877 – 886, 2008.

Other articles cited in this document

I. Aavatsmark, G. Eigestad, R. Klausen, M. Wheeler, and I. Yotov. Convergence of a symmetric MPFA method on quadrilateral grids. *Comput. Geosci.*, 11(4):333–345, 2007.

R. Abgrall and S. Tokareva. Staggered grid residual distribution scheme for Lagrangian hydrodynamics. *SIAM J. Sci. Comput.*, 39(5):A2317–A2344, 2017.

F. L. Addessio, J. R. Baumgardner, J. K. Dukowicz, N. L. Johnson, B. A. Kashiwa, R. M. Rauenzahn, and C. Zemach. CAVEAT: A Computer Code for Fluid Dynamics Problems with Large Distortion and Internal Slip. Technical report, Los Alamos National Laboratory LA-10613, 1990.

M. R. Baer and J. W. Nunziato. A two-phase mixture theory for the deflagration-to-detonatoin transition (DDT) in reactive granular materials. *Int. J. Multiphase Flow*, 12(6):861–889, 1986.

A. Barlow. A high order cell centred dual grid Lagrangian Godunov scheme. *Comput. Fluids*, 83: 15–24, 2013.

A. Barlow and P. Roe. A cell centred lagrangian godunov scheme for shock hydrodynamics. *Comput. Fluids*, 46(1):133–136, 2011.

A. Barlow, P.-H. Maire, W. Rider, R. Rieben, and M. Shashkov. Arbitrary Lagrangian-Eulerian methods for modeling high-speed compressible multimaterial flows. *J. Comput. Phys.*, 322:603 – 665, 2016a.

T. Barth and D. Jespersen. The design and application of uind schemes on unstructured meshes. in *aiaa paper 89-0366*. In *27th Aerospace Sciences Meeting*, Reno, Nevada, 1989b.

D. J. Benson. Computational methods in Lagrangian and Eulerian hydrocodes. *Comp. Meth. Appl. Mech. Eng.*, 99(2–3):235–394, 1992c.

C. Berthon and V. Desveaux. An entropy preserving MOOD scheme for the Euler equations. *Int. J. Finite Volumes*, 11, 2014.

E. Bertolazzi and G. Manzini. A second-order maximum principle preserving finite volume method for steady convection-diffusion problems. *SIAM J. Numer. Anal.*, 43(5):2172–2199 (electronic), 2005.

E. Bertolazzi and G. Manzini. On vertex reconstructions for cell-centered finite volume approximations of 2D anisotropic diffusion problems. *Math. Mod. Meth. Appl. Sci.*, 17:1–32, 2007b.

N. Bourago and V. Kukudzhanov. A review of contact algorithms. *Mechanics of Solids*, 40(1):35–71, 2005.

J.-P. Braeunig. Reducing the entropy production in a collocated Lagrange–Remap scheme. *J. Comput. Phys.*, 314:127–144, 2016.

J.-P. Braeunig and B. Chaudet. Study of a collocated Lagrange-remap scheme for multi-material flows adapted to HPC. *Int. J. Numer. Methods Fluids*, 83(8):664–678, 2017.

J. Breil and P.-H. Maire. A cell-centered diffusion scheme on two-dimensional unstructured meshes. *J. Comput. Phys.*, 224(2):785–823, 2007.

A. Bressan. *Hyperbolic systems of conservation laws*. Oxford University Press Inc., New York, NY, USA, 2000.

F. Brezzi, K. Lipnikov, and M. Shashkov. Convergence of the mimetic finite difference method for diffusion problems on polyhedral meshes. *SIAM J. Numer. Anal.*, 43(5):1872–1896, 2005.

F. Brezzi, A. Buffa, and K. Lipnikov. Mimetic finite differences for elliptic problems. *ESAIM, Math. Model. Numer. Anal.*, 43(2):277–295, 2009.

D. Burton. Exact conservation of energy and momentum in staggered-grid hydrodynamics with arbitrary connectivity. Technical Report UCRL-JC-105926, Lawrence Livermore National Laboratory, 1990.

D. Burton, T. Carney, N. Morgan, S. Sambastivan, and M. Shashkov. A cell-centered Lagrangian Godunov-like method for solid dynamics. *Comput. Fluids*, 83:33 – 47, 2013b.

D. Burton, N. Morgan, T. Carney, and M. Kenamond. Reduction of dissipation in Lagrange cell-centered hydrodynamics (CCH) through corner gradient reconstruction. *J. Comput. Phys.*, 299: 229 – 280, 2015a.

J.-S. Camier and F. Hermeline. A monotone nonlinear finite volume method for approximating diffusion operators on general meshes. *Int. J. Numer. Meth. Engng*, 107:496–519, 2016.

E. J. Caramana. The implementation of slide lines as a combined force and velocity boundary condition. *J. Comput. Phys.*, 228:3911–3916, 2009.

E. J. Caramana and M. J. Shashkov. Elimination of Artificial Grid Distortion and Hourglass-Type Motions by Means of Lagrangian Subzonal Masses and Pressures. *J. Comput. Phys.*, 142:521–561, 1998a.

E. J. Caramana, D. E. Burton, M. J. Shashkov, and P. P. Whalen. The construction of compatible hydrodynamics algorithms utilizing conservation of total energy. *J. Comput. Phys.*, 146:227–262, 1998b.

J. I. Castor. *Radiation Hydrodynamics*. Cambridge University Press, 2004.

S. Chandrasekhar. *Radiative transfer.* (International Series of Monographs on Physics) Oxford: Clarendon Press; London: Oxford University Press. XIV, 394 p. , 1950.

C.-H. Chang, X. Deng, and T. Theofanous. Direct numerical simulation of interfacial instabilities: a consistent, conservative, all-speed, sharp-interface method. *J. Comput. Phys.*, 242:946–990, 2013.

D. Chauveheid. A new algorithm for surface tension forces in the framework of the FVCF-ENIP method. *Eur. J. Mech. - B/Fluids*, 50:175–186, 2015.

J. Cheng and C.-W. Shu. A cell-centered Lagrangian scheme with the preservation of symmetry and conservation properties for compressible fluid flows in two-dimensional cylindrical geometry. *J. Comput. Phys.*, 229:7191–7206, 2010.

J. Cheng and C.-W. Shu. Positivity-preserving lagrangian scheme for multi-material compressible flow. *J. Comput. Phys.*, 257:143 – 168, 2014a.

F. Chopot. Couplage Euler/Navier-Stokes en 1D. Master's thesis, Université de Nantes, 2016.

P. Ciarlet. *The finite element method for elliptic problems.* SIAM, 2002b.

S. Clain, S. Diot, and R. Loubère. A high-order finite volume method for systems of conservation laws-Multi-dimensional Optimal Order Detection (MOOD). *J. Comput. Phys.*, 230(10):4028–4050, 2011.

J.-M. Clarisse, S. Jaouen, and P.-A. Raviart. A Godunov-type method in Lagrangian coordinates for computing linearly-perturbed planar-symmetric flows of gas dynamics. *J. Comput. Phys.*, 198 (1):80 – 105, 2004.

T. Corot and B. Mercier. A new nodal solver for the two dimensional Lagrangian hydrodynamics. *J. Comput. Phys.*, 353:1–25, 2018.

Y. Coudière, J.-P. Vila, and P. Villedieu. Convergence rate of a finite volume scheme for a two dimensional convection-diffusion problem. *Math. Model. Numer. Anal.*, 33(3):493–516, 1999.

N. Crouseilles and M. Lemou. An asymptotic preserving scheme based on a micro-macro decomposition for collisional Vlasov equations: diffusion and high-field scaling limits. *Kinetic and Related Models*, 4(2):441–477, 2011.

C. Dafermos. *Hyperbolic conservation laws in continuum physics.* Springer-Verlag, Heidelberg, Germany, 2000.

A. Danilov and Y. Vassilevski. A monotone nonlinear finite volume method for diffusion equations on conformal polyhedral meshes. *Russian J. Numer. Anal. Math. Modelling*, 24(3):207–227, 2009.

S. De Santis. Private Communication, 2011.

S. Del Pino. A curvilinear finite-volume method to solve compressible gas dynamics in semi-Lagrangian coordinates. *C.R. Acad. Sci.*, 348(17-18):1027–1032, 2010.

S. Del Pino. Metric-based mesh adaptation for 2d lagrangian compressible flows. *J. Comput. Phys.*, 230(5):1793–1821, 2011.

S. Dellacherie. Analysis of Godunov type schemes applied to the compressible Euler system at low Mach number. *J. Comput. Phys.*, 229:978–1016, 2010.

B. Després. Lagrangian systems of conservation laws. *Numerische Mathematik*, 89(1):99–134, Jul 2001.

B. Després. Weak consistency of the cell-centered Lagrangian GLACE scheme on general meshes in any dimension. *Comp. Meth. Appl. Mech. Eng.*, 199:2669–2679, 2010c.

B. Després. *Numerical methods for Eulerian and Lagrangian conservation laws.* Birkhauser, 2017.

B. Després and C. Mazeran. Symmetrization of Lagrangian gas dynamics and Lagrangian solvers. *C.R. Acad. Sci.*, 331:475–480, 2003.

B. Després and C. Mazeran. Lagrangian Gas Dynamics in Two Dimensions and Lagrangian systems. *Arch. Rational Mech. Anal.*, 2005.

V. A. Dobrev, T. V. Kolev, and R. N. Rieben. High-order curvilinear finite element methods for Lagrangian hydrodynamics. *SIAM J. Sci. Comput.*, 34(5):B606–B641, 2012.

J. Droniou and C. Le Potier. Construction and convergence study of schemes preserving the elliptic local maximum principle. *SIAM J. Numer. Anal.*, 49(2):459–490, 2011.

J. Droniou, R. Eymard, T. Gallouët, and R. Herbin. A unified approach to mimetic finite difference, hybrid finite volume and mixed finite volume methods. *Math. Mod. Meth. Appl. Sci.*, 2009.

J. Droniou, R. Eymard, T. Gallouët, and R. Herbin. A unified approach to mimetic finite difference, hybrid finite volume and mixed finite volume methods. *Math. Mod. Meth. Appl. Sci.*, 20(2): 265–295, 2010.

J. Droniou, R. Eymard, and R. Herbin. Gradient schemes: generic tools for the numerical analysis of diffusion equations. *Math. Model. Numer. Anal.*, 50:749–781, 2016.

J. Droniou, R. Eymard, T. Gallouët, C. Guichard, and R. Herbin. *The gradient discretisation method*, volume 82. Springer, 2018.

M. Edwards and C. Rogers. Finite volume discretization with imposed flux continuity for the general tensor pressure equation. *Comput. Geosci.*, 2:259–290, 1998.

M. G. Edwards and H. Zheng. A quasi-positive family of continuous Darcy-flux finite-volume schemes with full pressure support. *J. Comput. Phys.*, 227(22):9333–9364, 2008.

G. T. Eigestad, I. Aavatsmark, and M. Espedal. Symmetry and M-matrix issues for the O-method on an unstructured grid. *Comput. Geosci.*, 6(3-4):381–404, 2002. Locally conservative numerical methods for flow in porous media.

C. Enaux. *Analyse mathématique et analyse numérique d'un modèle d'interpénétration de plasmas.* PhD thesis, École Centrale de Paris, 2007.

J. Escobar, E. Rodríguez, R. Montenegro, G. Montero, and J. González-Yuste. Simultaneous untangling and smoothing of tetrahedral meshes. *Comput. Methods Appl. Mech. Eng.*, 192(25):2775 – 2787, 2003.

L. Evans. Application of nonlinear semigroup theory to certain partial differential equations. *Nonlinear Evolution Equations*, pages 163–188, 1978.

R. Eymard, T. Gallouët, and R. Herbin. Discretization of heterogeneous and anisotropic diffusion problems on general nonconforming meshes SUSHI: A scheme using stabilization and hybrid interfaces. *IMA J. Numer. Anal.*, 30(4):1009–1043, 2010.

C. Farhat, P. Geuzaine, and C. Grandmont. The Discrete Geometric Conservation Law and the Nonlinear Stability of ALE Schemes for the Solution of Flow Problems on Moving Grids. *J. Comput. Phys.*, 174(2):669 – 694, 2001.

S. Fechter, C.-D. Munz, C. Rohde, and C. Zeiler. Approximate Riemann solver for compressible liquid vapor flow with phase transition and surface tension. *Comput. Fluids*, 169:169–185, 2018.

R. Fedkiw, T. Aslam, B. Merriman, and S. Osher. A non-oscillatory Eulerian approach to interfaces in multimaterial flows (the ghost fluid method). *J. Comput. Phys.*, 152(2):457–492, 1999.

D. P. Flanaghan and T. Belytshko. A uniform strain hexaedron and quadrilateral and orthogonal hourglass control. *Int. J. Numer. Meth. Engrg.*, 17:679–706, 1982b.

L. A. Freitag and P. E. Plassman. Local optimization-based untangling algorithms for quadrilateral meshes. *Int. J. Numer. Methods Eng.*, 49:109–125, 2000b.

H. Frid. Maps of convex sets and invariant regions for finite-difference systems of conservation laws. *Arch. Ration. Mech. Anal.*, 160(3):245–269, 2001.

H. A. Friis and M. G. Edwards. A family of MPFA finite-volume schemes with full pressure support for the general tensor pressure equation on cell-centered triangular grids. *J. Comput. Phys.*, 230 (1):205–231, 2011.

D. Fuster and S. Popinet. An all-Mach method for the simulation of bubble dynamics problems in the presence of surface tension. *J. Comput. Phys.*, 374:752–768, 2018.

G. Gallice. Positive and Entropy stable Godunov-type Schemes for Gas Dynamics and MHD Equations in Lagrangian or Eulerian Coordinates. *Numerische Mathematik*, 4:673–713, Jun 2003.

D. Garrick, M. Owkes, and J. Regele. A finite-volume HLLC-based scheme for compressible interfacial flows with surface tension. *J. Comput. Phys.*, 339:46–67, 2017.

G. Georges, J. Breil, and P.-H. Maire. A 3D GCL compatible cell-centered Lagrangian scheme for solving gas dynamics equations. *J. Comput. Phys.*, 305:921–941, 2016.

E. Godlewski and P.-A. Raviart. *Numerical Approximation of Hyperbolic Systems of Conservation Laws*. Applied Mathematical Sciences 118. Springer, 1995.

S. Godunov. *Different Methods for Shock Waves*. PhD thesis, Moscow State University, 1954.

S. Godunov. A differerence scheme for numerical computation of discontinuous solution of hydrodynamic equations. *Math. Sib.*, 47, 1959.

R. Goldman. Curvature formulas for implicit curves and surfaces. *Computer Aided Geometric Design*, 22(7):632 – 658, 2005. Geometric Modelling and Differential Geometry.

S. Gottlieb, C.-W. Shu, and E. Tadmor. Strong stability-preserving high-order time discretization methods. *SIAM review*, 43(1):89–112, 2001.

J.-L. Guermond, M. Nazarov, B. Popov, and I. Tomas. Second-order invariant domain preserving approximation of the Euler equations using convex limiting. *SIAM J. Sci. Comput.*, 40(5):A3211–A3239, 2018.

F. Hermeline. A finite volume method for second-order elliptic equations. (Une méthode de volumes finis pour les équations elliptiques du second ordre.). *C. R. Acad. Sci. Paris, Ser. I*, 1998.

F. Hermeline. A finite volume method for the approximation of diffusion operators on distorted meshes. *J. Comput. Phys.*, 160(2):481–499, 2000.

F. Hermeline. Approximation of diffusion operators with discontinuous tensor coefficients on distorted meshes. *Comput. Methods Appl. Mech. Eng.*, 192(16-18):1939–1959, 2003.

F. Hermeline. Approximation of 2D and 3D diffusion operators with variable full tensor coefficients on arbitrary meshes. *Comput. Methods Appl. Mech. Eng.*, 196(21-24):2497–2526, 2007.

F. Hermeline. *Nouvelles méthodes de volumes finis pour approcher des équations aux dérivées partielles sur des maillages quelconques*. Habilitation à diriger des recherches, CEA/DAM Ile de France, 2008.

F. Hermeline. A finite volume method for approximating 3D diffusion operators on general meshes. *J. Comput. Phys.*, 228(16):5763–5786, 2009.

J. Hervé. Stabilité et limitation réalisable pour des quantités tensorielles. Master's thesis, Université de Nantes, 2016.

C. Hirt and B. Nichols. Volume of fluid (vof) method for the dynamics of free boundaries. *J. Comput. Phys.*, 39(1):201–225, 1981.

P. Hoch. An arbitrary Lagrangian-Eulerian strategy to solve compressible flows. *H. A. L.*, hal-00366858, 2009.

S. Jaouen and F. Lagoutière. Numerical transport of an arbitrary number of components. *Comput. Methods Appl. Mech. Eng.*, 196(33-34):3127–3140, 2007.

I. Kataoka. Local instant formulation of two-phase flow. *Int. J. Multiphase Flow*, 12(5):745 – 758, 1986.

D. S. Kershaw. Differencing of the diffusion equation in Lagrangian hydrodynamic codes. *J. Comput. Phys.*, 39:375–395, 1981.

G. Kluth. *Analyse mathématique et numérique de systèmes hyperélastiques et introduction à la plasticité*. PhD thesis, Université Pierre et Marie Curie, 2008.

G. Kluth and B. Després. Discretization of hyperelasticity on unstructured mesh with a cell-centered Lagrangian scheme. *J. Comput. Phys.*, 2010.

P. M. Knupp. Achieving finite element mesh quality via optimization of the Jacobian matrix norm and associated quantities. Part II-a framework for volume mesh optimization and the condition number of the Jacobian matrix. *Int. J. Numer. Methods Eng.*, 48(8):1165–1185, 2000b.

P. M. Knupp. Achieving finite element mesh quality via optimization of the Jacobian matrix norm and associated quantities. Part I-a framework for surface mesh optimization. *Int. J. Numer. Methods Eng.*, 48(3):401–420, 2000c.

M. Kucharick, R. Loubère, L. Bednárik, and R. Liska. Enhancement of Lagrangian Slide Lines as a Combined Force and Velocity Boundary Condition. *Comput. Fluids*, 2012.

Y. Kuznetsov, K. Lipnikov, and M. Shashkov. The mimetic finite difference method on polygonal meshes for diffusion-type problems. *Comput. Geosci.*, 8(4):301–324, 2005.

P. Lax and B. Wendroff. Systems of conservation laws. *Comm. Pure Appl. Math.*, 13:381–398, 1960.

C. Le Potier. A linear scheme satisfying a maximum principle for anisotropic diffusion operators on distorted grids. (Un schéma linéaire vérifiant le principe du maximum pour des opérateurs de diffusion très anisotropes sur des maillages déformés.). *C. R., Math., Acad. Sci. Paris*, 347(1-2): 105–110, 2009.

R. J. Leveque. *Finite volume methods for hyperbolic problems*. Cambridge Texts in Applied Mathematics. Cambridge university Press, 2002.

Z. Li, X. Yu, and Z. Jia. The cell-centered discontinuous Galerkin method for Lagrangian compressible Euler equations in two-dimensions. *Comput. Fluids*, 96:152 – 164, 2014.

K. Lipnikov, M. Shashkov, and D. Svyatskiy. The mimetic finite difference discretization of diffusion problem on unstructured polyhedral meshes. *J. Comput. Phys.*, 211(2):473–491, 2006.

K. Lipnikov, M. Shashkov, D. Svyatskiy, and Y. Vassilevski. Monotone finite volume schemes for diffusion equations on unstructured triangular and shape-regular polygonal meshes. *J. Comput. Phys.*, 227(1):492–512, 2007.

K. Lipnikov, D. Svyatskiy, and Y. Vassilevski. Interpolation-free monotone finite volume method for diffusion equations on polygonal meshes. *J. Comput. Phys.*, 228(3):703–716, 2009b.

K. Lipnikov, D. Svyatskiy, and Y. Vassilevski. A monotone finite volume method for advection-diffusion equations on unstructured polygon meshes. *J. Comput. Phys.*, 229(11):4017–4032, 2010.

K. Lipnikov, G. Manzini, and D. Svyatskiy. Monotonicity conditions in the mimetic finite difference method. In *Finite volumes for complex applications. VI. Problems & perspectives. Volume 1, 2*, volume 4 of *Springer Proc. Math.*, pages 653–661. Springer, Heidelberg, 2011.

K. Lipnikov, D. Svyatskiy, and Y. Vassilevski. Minimal stencil finite volume scheme with the discrete maximum principle. *Russian J. Numer. Anal. Math. Modelling*, 27(4):369–385, 2012.

K. Lipnikov, G. Manzini, and M. Shashkov. Mimetic finite difference method. *J. Comput. Phys.*, 257, Part B(0):1163 – 1227, 2014a. Physics-compatible numerical methods.

X. Liu, N. Morgan, and D. Burton. A Lagrangian discontinuous Galerkin hydrodynamic method. *Comput. Fluids*, 163:68–85, 2018a.

X. Liu, N. Morgan, and D. Burton. Lagrangian discontinuous Galerkin hydrodynamic methods in axisymmetric coordinates. *J. Comput. Phys.*, 373:253–283, 2018b.

Y. Liu, W. Shen, B. Tian, and D.-K. Mao. A two dimensional nodal Riemann solver based on one dimensional Riemann solver for a cell-centered Lagrangian scheme. *J. Comput. Phys.*, 284:566 – 594, 2015.

A. Llor, A. Claisse, and C. Fochesato. Energy preservation and entropy in lagrangian space- and time-staggered hydrodynamic schemes. *J. Comput. Phys.*, 309:324 – 349, 2016.

R. Loubère, P.-H. Maire, and B. Rebourcet. Chapter 13 - Staggered and colocated finite volume schemes for Lagrangian hydrodynamics. In R. Abgrall and C.-W. Shu, editors, *Handbook of Numerical Methods for Hyperbolic Problems*, volume 17 of *Handbook of Numerical Analysis*, pages 319 – 352. Elsevier, 2016.

G. Luttwak and J. Falcovitz. Slope limiting for vectors: a novel vector limiting algorithm. *Int. J. Numer. Meth. Fluids*, 65:1365–1375, 2011a.

P.-H. Maire. A high-order cell-centered Lagrangian scheme for compressible fluid flows in two-dimensional cylindrical geometry. *J. Comput. Phys.*, 228(18):6882–6915, 2009b.

P.-H. Maire. A high-order cell centered lagrangian scheme for two-dimensional compressible fluid flows on unstructured meshes. *J. Comput. Phys.*, 228(7):2391–2425, 2009c.

P.-H. Maire. *Contribution to the numerical modeling of inertial confinement fusion.* CEA/DAM, Mars 2011b. CEA-R-6260.

P.-H. Maire, R. Abgrall, J. Breil, and J. Ovadia. A cell-centered Lagrangian scheme for two-dimensional compressible flow problems. *SIAM J. Sci. Comput.*, 29(4):1781–1824, 2007b.

C. Mazeran. *Sur la structure mathématique et l'approximation numérique de l'hydrodynamique Lagrangienne bidimensionelle.* PhD thesis, Université Bordeaux I, 2007b.

D. Mihalas and B. Weibel-Mihalas. *Foundations of radiation hydrodynamics.* Dover, New York, NY, USA, 1999.

N. Morgan, J. Waltz, D. Burton, M. Charest, T. Canfield, and J. Wohlbier. A point-centered arbitrary Lagrangian Eulerian hydrodynamic approach for tetrahedral meshes. *J. Comput. Phys.*, 290:239 – 273, 2015.

J. v. Neumann and R. D. Richtmyer. A method for the calculation of hydrodynamics shocks. *J. appl. Phys.*, 21:232–237, 1950b.

N. T. Nguyen and M. Dumbser. A path-conservative finite volume scheme for compressible multi-phase flows with surface tension. *Applied Mathematics and Computation*, 271:959–978, 2015.

K. Nikitin and Y. Vassilevski. A monotone nonlinear finite volume method for advection-diffusion equations on unstructured polyhedral meshes in 3D. *Russian J. Numer. Anal. Math. Modelling*, 25(4):335–358, 2010.

S. Osher, R. Fedkiw, and K. Piechor. Level set methods and dynamic implicit surfaces. *Appl. Mech. Rev.*, 57(3):B15–B15, 2004.

C. Paulin, J.-P. Braeunig, and R. Motte. Isentropic correction for collocated Lagrange-Remap scheme. *Comput. Math. Appl.*, 78(2):623 – 642, 2019.

G. Perigaud and R. Saurel. A compressible flow model with capillary effects. *J. Comput. Phys.*, 209 (1):139 – 178, 2005.

G. J. Pert. Physical constraints in numerical calculations of diffusion. *J. Comput. Phys.*, 42(1): 20–52, 1981.

B. Perthame and C.-W. Shu. On positivity preserving finite volume schemesfor Euler equations. *Numerische Mathematik*, 73(1):119–130, Mar 1996.

G. C. Pomraning. The non-equilibrium Marshak wave problem. *J. Quant. Spectrosc. Radiat.*, 21(3): 249 – 261, 1979.

A. Rambaud. Un schéma "Asymptotic Preserving" et "Well-Balanced" pour le rayonnement couplé à la matière. Master's thesis, Mines de Nancy, 2016.

R. D. Richtmyer. Taylor instability in shock acceleration of compressible fluids. *Comm. Pure Appl. Math.*, 13(297), 1960b.

C. Rohde and C. Zeiler. A relaxation Riemann solver for compressible two-phase flow with phase transition and surface tension. *Appl. Numer. Math.*, 95:267–279, 2015.

A. J. Scannapieco and B. Cheng. A multifluid interpenetration mix model. *Phys. Lett. A 299*, pages 49–64, 2002.

K. Schmidmayer, F. Petitpas, E. Daniel, N. Favrie, and S. Gavrilyuk. A model and numerical method for compressible flows with capillary effects. *J. Comput. Phys.*, 334:468 – 496, 2017.

R. Sentis. *Mathematical Models and Methods for Plasma Physics, Volume 1: Fluid Models*. Springer Science & Business Media, 2014.

D. Serre. Domaines invariants pour les systèmes hyperboliques de lois de conservation. *J. Differential Equations*, 69(1):46–62, 1987.

Z. Sheng and G. Yuan. The finite volume scheme preserving extremum principle for diffusion equations on polygonal meshes. *J. Comput. Phys.*, 230(7):2588–2604, 2011.

Z. Sheng, J. Yue, and G. Yuan. Monotone finite volume schemes of nonequilibrium radiation diffusion equations on distorted meshes. *SIAM J. Sci. Comput.*, 31(4):2915–2934, 2009.

V. Siess. A linear and accurate diffusion scheme respecting the maximum principle on distorted meshes. *C. R. Acad. Sci. Paris, Ser. I*, 347:1317–1320, 2009.

C. Sijoy and S. Chaturvedi. An Eulerian multi-material scheme for elastic-plastic impact and penetration problems involving large material deformations. *Eur. J. Mech. B Fluids*, 53:85 – 100, 2015.

C. Sijoy and S. Chaturvedi. TRHD: Three-temperature radiation-hydrodynamics code with an implicit non-equilibrium radiation transport using a cell-centered monotonic finite volume scheme on unstructured-grids. *Phys. Comm.*, 190:98 – 119, 2016.

Y. Sun, M. Yu, Z. Jia, and Y.-X. Ren. A cell-centered Lagrangian method based on local evolution Galerkin scheme for two-dimensional compressible flows. *Comput. Fluids*, 128:65 – 76, 2016.

P. D. Thomas and C. K. Lombard. Geometric conservation law and its application to flow computations on moving grids. *AIAA J.*, 17(10):1030–1037, 1979.

E. F. Toro. *Riemann solvers and numerical methods for fluid dynamics*. Springer, 1997.

J. Trulio and K. Trigger. Numerical solution of the one-dimensional Lagrangian hydrodynamic equations. Technical Report UCRL-6267, Lawrence Radiation Laboratory, 1961.

G. Tryggvason, B. Bunner, A. Esmaeeli, D. Juric, N. Al-Rawahi, W. Tauber, J. Han, S. Nas, and Y.-J. Jan. A front-tracking method for the computations of multiphase flow. *J. Comput. Phys.*, 169(2):708–759, 2001.

S. Unverdi and G. Tryggvason. A front-tracking method for viscous, incompressible, multi-fluid flows. *J. Comput. Phys.*, 100(1):25–37, 1992.

P. Vachal, R. V. Garimella, and M. J. Shashkov. Untangling of 2D meshes in ALE simulations. *J. Comput. Phys.*, 196:627–644, 2003a.

B. van Leer. Towards the ultimate conservative difference scheme V. A second order sequel to Godunov's method. *J. Comput. Phys.*, 32(101–136), 1979.

F. Vilar. *Utilisation des méthodes de Galerkin discontinues pour la résolution de l'hydrodynamique Lagrangienne bi-dimensionnelle*. PhD thesis, Université Bordeaux I, 2012.

F. Vilar, P.-H. Maire, and R. Abgrall. A discontinuous Galerkin discretization for solving the two-dimensional gas dynamics equations written under total Lagrangian formulation on general unstructured grids. *J. Comput. Phys.*, 276:188 – 234, 2014.

F. Vilar, C.-W. Shu, and P.-H. Maire. Positivity-preserving cell-centered Lagrangian schemes for multi-material compressible flows: From first-order to high-orders. Part II: The two-dimensional case. *J. Comput. Phys.*, 312:416 – 442, 2016a.

S. Wang, G. Yuan, Y. Li, and Z. Sheng. A monotone finite volume scheme for advection-diffusion equations on distorted meshes. *Internat. J. Numer. Methods Fluids*, 69(7):1283–1298, 2012.

M. L. Wilkins. Calculation of Elastic-Plastic Flow. In *Methods in Computational Physics*, volume 3, pages 211–263. Accademic Press, 1964b.

A. M. Winslow. Numerical solution of the quasilinear Poisson equation in a nonuniform triangle mesh. *J. Comput. Phys.*, 1(2):149–172, 1966.

G. Yuan and Z. Sheng. Monotone finite volume schemes for diffusion equations on polygonal meshes. *J. Comput. Phys.*, 227(12):6288–6312, June 2008.

Y. B. Zel'dovich and Y. P. Raizer. Physics of Shock Waves and High-Temperature Hydrodynamic Phenomena. *Academic Press*, 1966.

X. Zhang and C.-W. Shu. On maximum-principle-satisfying high order schemes for scalar conservation laws. *J. Comput. Phys.*, 229(9):3091 – 3120, 2010.